STUDY ON THE CHARACTERISTICS AND RESPONSE CONTROL EFFECTS OF A SEISMIC MASS DAMPER SYSTEM UTILIZING SCRAP TIRE PADS

by

PARK JI HYUN

A dissertation

submitted to the Hokkaido University

in partial fulfilment of the requirement for the degree of

Doctor of Philosophy

in the field of Architectural and Structural Design

January 31, 2023

北海道大学
HOKKAIDO UNIVERSITY

ACKNOWLEDGMENTS

First of all, I would like to express my deep gratitude to my supervisor, Dr. Kazutaka SHIRAI, an associate professor at Hokkaido University, who provided me with daily consultations and guidance that enabled me to move my research forward step by step. He gave me a lot of help right up to the end, offering good directions for my research, and his many times of careful consultation helped me to resolve my doubts and motivated me to work on my research. I am sincerely and deeply grateful for his patience, teachings and heartfelt advice he gave me during my Ph.D. years.

I further express our gratitude to my thesis committee members, Dr. Taichiro OKAZAKI and Dr. Shunji KANIE. Their advice helped me to think about directions in which I should be more diligent, while enlightening me to various points of view. I am also grateful to Professor Masaru KIKUCHI at Hokkaido University for providing great support and environment at the Building Structure Control Laboratory.

I would appreciate to Dr. Hideaki Kato and Dr. Masahiro Nakamura of Bridgestone Corporation for conducting the experiments. And I would also like to thank Japan Meteorological Agency and Building Performance Standardization Association for providing the data used in the analysis in this study. This study was supported by the Japan Society for the Promotion of Science, KAKENHI Grant number 16K14180.

I would like to extend my sincere regards to Emi KIRIMOTO for helping me with the official paperwork throughout my study. And thank you for completing the thesis with the help of all the lab members, including Bote SHU, Sonia LONGJAM, Marco GREGORIUS and Ruomin ZHANG.

I am indescribably grateful to my beloved family and friends for their endless encouragement and support throughout my study life. And thank you to all those who helped me that I could not mention yet.

Finally, I would like to thank the University of Hokkaido for helping me proceed with this paper.

ABSTRACT

As environmental problems have emerged, attempts have been made to use waste as a building material. Recent studies have proposed and investigated vibration control techniques, including seismic isolation and tuned mass damper systems for earthquakes using waste or used tires. Amid these flows, more recently, a seismic mass damper (SMD) system using scrap tire pads (STPs) for building structures has been proposed. The STP unit can be made by cutting the tread part of radial tires and laminating multilayers. In the SMD system, an adequate number of STPs are placed in the vibration control story at the top of the mainframe of a superstructure to exert a mass damper effect during an earthquake. It is expected that STPs act as the necessary spring, damper, and bearing functions for the SMD system. The system is expected to mitigate the peak responses of a building structure during an earthquake, resulting in a reduction of the damage to humans, structures, and non-structural members. The reuse of tires for STPs contributes to the solution of environmental problems such as excessive waste generation. Although past studies proposed various systems including base-isolated structures using waste or used tires and investigated the characteristics through experiments, no studies on the SMD systems using STPs have been conducted. No dynamic loading tests on STPs were conducted except for free vibration tests, thus the dynamic behavior of STPs for various parameters including the loading amplitude and speed, and surface pressure effects has not been clarified yet. In addition, the vibration control effects of the SMD system utilizing STPs subjected to seismic motions have not been examined.

This dissertation aimed to grasp the availability of the SMD system using STPs for seismic response reduction of buildings. The following specific objectives were examined for this goal: (1) to investigate the mechanical behavior of STPs under horizontal and vertical loadings through experiments; (2) to assess the performance of STPs concerning horizontal stiffness and damping characteristics; (3) to numerically evaluate the control effects of the SMD using STPs by earthquake response analyses. In this research, loading tests using STP unit specimens were conducted to understand the mechanical characteristics of STPs. Additionally, to evaluate the effectiveness of the SMD system, seismic response simulation was performed under various input motions using the mechanical properties obtained from the experiments.

TABLE OF CONTENTS

LIST OF FIGURES

LIST OF TABLES

LIST OF SYMBOLS

A horizontal area of each STP unit specimen

C_d total lateral damping coefficient of the mass damper story

$C_{2,M05A}$ total lateral viscous damping coefficient of the vibration control story for Case M05A

$C_{2,M05B}$ total lateral viscous damping coefficient of the vibration control story for Case M05B

$C_{2,M05C}$ total lateral viscous damping coefficient of the vibration control story for Case M05C

$C_{2,M05D}$ total lateral viscous damping coefficient of the vibration control story for Case M05D

$C_{2,M05E}$ total lateral viscous damping coefficient of the vibration control story for Case M05E

Δ_1 displacements corresponding and F_1

Δ_2 displacements corresponding and F_2

ΔW energy loss

E_v vertical equivalent Young's modulus

F_1 minimum vertical load

F_2 maximum vertical load

h_{eq} horizontal equivalent viscous damping factor

$h_{eq,STP}$ horizontal equivalent viscous damping factor of STP unit

K_d total lateral stiffness of mass damper story

K_{eq} horizontal equivalent stiffness

$K_{eq,STP}$ horizontal equivalent stiffness of STP unit

K_v vertical equivalent stiffness

K_1 initial stiffness

K_2 stiffness after cracking

K_3 stiffness after yielding

$K_{2,M05A}$ total lateral stiffness of the vibration control story for Case M05A

$K_{2,M05B}$ total lateral stiffness of the vibration control story for Case M05B

$K_{2,M05C}$ total lateral stiffness of the vibration control story for Case M05C

$K_{2,M05D}$ total lateral stiffness of the vibration control story for Case M05D

$K_{2,M05E}$ total lateral stiffness of the vibration control story for Case M05E

M_d the mass of the SMD additional mass

M_1 mass of main structure

M_2 mass of additional mass

N_d required number of STP units

Q_{max} maximum force

Q_{min} minimum force

Q_1 shear force at the cracking point

Q_2 shear force at the yielding point

t overall thickness

W potential deformation energy of K_{eq}

X_{max} maximum displacement

X_{min} minimum displacement

μ_{eff} ratio of the SMD additional mass to the first modal effective mass of the superstructure

μ_{total} ratio of the SMD additional mass to the total mass of the superstructure

ν_{opt} where ν_{opt} is the optimal frequency ratio for the natural frequency of the mass damper alone to the first modal natural frequency of the building without an SMD

Chapter I

Introduction

Chapter I includes the contents of the following published papers.

Shirai K, Park J, "Use of scrap tire pads in vibration control system for seismic response reduction of buildings", Bulletin of Earthquake Engineering, 18(5), 2497–2521, 2020.

Introduction

1. Research background

As environmental problems have emerged, attempts have been made to use waste as a building material. In recent years, seismic isolation systems using waste tires have been studied. Taking advantage of waste tires is expected to reduce the environmental impact and cost owing to the recycling of materials. Shinba and Fujii (2003; 2004) proposed a housing sliding base isolation system that incorporated waste tires instead of bearings as horizontal springs. They assumed the use of whole tires without cutting them and conducted compression tests and earthquake response analyses on whole tires. Ueda and Ohba (2005) studied on a low-cost base isolation system using rubber pulverized to powder form, which was a recycled material made from waste tires. They proposed to fill the side trench of a sliding base isolation system with the rubber powder to form horizontal cushioning elements, and they conducted shaking table tests.

More recently, Turer and Özden (2008) proposed low-cost seismic isolation pads using scrap tire pads (STPs). They manufactured several laminated rubber sheet specimens by cutting up used tires from automobiles. They conducted axial compression tests, small-displacement free vibration tests, and large-displacement static shear loading tests. The mechanical and dynamic properties of the STP specimens made from different tire brands, numbers of layers, and layer orientations were experimentally evaluated. Mishra and Igarashi (2012), Mishra et al. (2012; 2013), and Igarashi et al. (2013) conducted experimental and numerical studies on STPs with unbonded or bonded layers for seismic isolation structures. They conducted vertical compression tests and horizontal loading tests using STP specimens, unidirectional tensile test using a dog-bone shape specimen, and pyrolysis gas chromatography analysis to investigate the mechanical and material properties of STPs. They also conducted finite element analysis and

compared the results with the tests. Mishra et al. (2014) conducted pseudo-dynamic tests for seismic performance assessment of a seismic isolation system using STPs. Reyna et al. (2018) used STPs in a similar way and studied a seismic isolator using recycled tire sheets. They conducted free vibration tests, horizontal loading tests under vertical pressures, and numerical analysis.

Conventionally, tuned mass dampers (TMDs) are one of the vibration suppression technologies used to decrease the response of structural systems under dynamic excitation. A typical TMD consists of a mass, spring, and viscous damping element attached to a vibrating system, such as the top of a structure. Much research on TMDs has been conducted for investigating their effectiveness and application since the 20th century (e.g., Den Hartog 1956), and it continues today (e.g., Fang et al. 2019; Wang et al. 2019). In recent decades, use of TMDs for seismic protection of buildings and civil structures has been studied (e.g., Sadek et al. 1997; Miranda 2005; Hoang et al. 2008). More recently, Kaneko (2018) has studied on the response control effects of a hysteresis-type TMD system installed at the top of a building structure model with nonlinear restoring force characteristics subjected to earthquakes. Nakai et al. (2019) have reported an application of seismic retrofitting for an existing high-rise building using large TMDs, whose total weight was planned to be equal to 6.5% of the effective building weight.

A number of recent studies have shown the proposals of the systems using tire pads and the characteristics of materials through experiments. However, Few extensive studies on STPs, especially for seismic response control systems have been conducted to date excluding the studies on base isolation. Moreover, no dynamic loading tests on STPs were conducted except for the free vibration tests and so that the dependence of STP behavior on various parameters, including the amplitude and velocity of dynamic loadings and surface pressure effects, have not been addressed. In addition, the vibration

control effects under earthquakes motions of the damper system utilizing STPs were not numerically verified. Therefore, experimental study on the mechanical properties of STPs and numerical evaluation of the control effects by the mass damper system using STPs are needed.

2. Objectives

The present study mainly aims to figure out the availability of the vibration control system using tires for seismic response reduction of buildings. There are four specific objectives to achieve this aim:

(1) To investigate the mechanical behaviour of STPs through experiments
(2) To assess the performance of STP units including the horizontal equivalent stiffness and damping factor
(3) To analyze the earthquake response behavior of buildings with a seismic mass damper (SMD) system using STPs
(4) To evaluate the response control effects achieved by the SMD system using STPs subjected to strong earthquakes

3. Methodology

In this study, the research methodology consisted of:
(1) Designing of STP specimens and conducting loading tests on STP specimens.
(2) Investigating the mechanical properties of STPs based on the obtained test results.
(3) Performing seismic response analysis on simplified linear building models with the SMD system using STPs and evaluating the effectiveness of the proposed system.
(4) Analyzing seismic response for nonlinear building models with the SMD system using STP and verifying the effectiveness of dampers.

4. Overview

The present thesis, including the introductory chapter, contains the contents of the following papers:
Paper I: Shirai K, Park J (2020) Use of scrap tire pads in vibration control system for seismic response reduction of buildings, Bulletin of Earthquake Engineering, 18(5), 2497–2521.
Paper II: Park J, Shirai K, Kikuchi M (2022) A seismic mass damper system using scrap tire pads: Loading tests on mechanical properties and numerical assessment of the response control effects, Soil Dynamics and Earthquake Engineering, vol. 157, 107257.

This dissertation is structured into six chapters as follows.

Chapter I is the introductory chapter. This chapter clarifies the research background on STPs and seismic damper system, objectives, and methodology.

Chapter II describes the mass damper system using the STP proposed in and reviewed in the study. It included an overview of the proposed system, advantages, and a brief estimate of the number of tires required to be applied to the actual building.

Chapter III demonstrates the mechanical properties of scrap tire pads experimentally. In the experiment, four types of test specimens were made with tires with different service life and manufacturer, and loading experiments were conducted with them. The loading test results indicated the dependence of repeat cycles, frequency, amplitude, surface pressure, and other mechanical properties, depending on the condition and manufacturer. All the STP specimens showed similar tendencies in their dependence on these parameters, although there were small differences depending on the status and manufacturer of the tires. The results demonstrated that the STP alone has a certain damping performance.

Chapter IV addresses seismic response analysis using a simplified linear model to determine the availability of STP as a mass damper. A numerical

two-degree-of-freedom (2DOF) building mainframe model was used to simulate the response of the proposed SMD system. The results of the analysis based on the presence or absence of a mass damper showed the effectiveness of the mass damper system using STPs.

Chapter V identifies STP performance as a mass damper by numerical analysis of the nonlinear multi-degree-of-freedom (MDOF) models. The analysis models were prepared by referring to two building models, a six-story reinforced-concrete building and a 10-story steel-reinforced-concrete building, which take into account soil-structure interactions. An earthquake response simulation was conducted with and without the SMD system using STPs. Response analysis showed that the maximum response acceleration of the superstructures in the controlled model has been clearly reduced compared to the uncontrolled model. Results revealed that the earthquake response is effectively reduced by setting the lateral stiffness and damping coefficient for the mass damper story to be smaller than those corresponding to the elastic natural period, in consideration of decreasing the equivalent stiffness of the main frame due to the progress of damage and plasticity.

Chapter VI is the conclusion of this entire study. This chapter also lists some recommendations for future studies.

5. Information details of the published papers

Peer reviewed conference paper:

Park J, Shirai K, Kikuchi M (2020) A seismic mass damper using scrap tire pads: experiment on mechanical property and analysis of control effect. The 17th World Conference on Earthquake Engineering, Sendai, Japan.

Published peer reviewed journal paper:

Park J, Shirai K, Kikuchi M (2022) A seismic mass damper system using scrap tire pads: Loading tests on mechanical properties and numerical assessment of the response control effects, Soil Dynamics and Earthquake Engineering, vol. 157, 107257.
https://doi.org/10.1016/j.soildyn.2022.107257

Shirai K, Park J (2020) Use of scrap tire pads in vibration control system for seismic response reduction of buildings, Bulletin of Earthquake Engineering, 18(5), 2497–2521.
https://doi.org/10.1007/s10518-020-00787-2

References

[1] Den Hartog JP (1956) Mechanical vibrations (4th ed.), McGraw-Hill, New York.

[2] Fang H, Liu L, Zhang D, Wen M (2019) Tuned mass damper on a damped structure, Structural Control and Health Monitoring, 26(3), e2324. https://doi.org/10.1002/stc.2324

[3] Hoang N, Fujino Y, Warnitchai P (2008) Optimal tuned mass damper for seismic applications and practical design formulas, Engineering Structures, 30(3), 707-715. https://doi.org/10.1016/j.engstruct.2007.05.007

[4] Igarashi A, Matsushima H, Mishra HK (2013) Investigation of material properties and shear deformation capacity of scrap tire rubber pad isolators, Journal of Japan Society of Civil Engineers, A1, 69(4), 958-964. (in Japanese) https://doi.org/10.2208/jscejseee.69.I_958

[5] Kaneko K (2018) Tuning strategy of hysteretic mass damper for reducing inter-story drift beyond elastic limit of steel buildings, Journal of Structural and Construction Engineering (Transactions of AIJ), 83(752), 1423-1433. (in Japanese) https://doi.org/10.3130/aijs.83.1423

[6] Miranda JC (2005) On tuned mass dampers for reducing the seismic response of structures, Earthquake Engineering and Structural Dynamics, 34(7), 847-865. https://doi.org/10.1002/eqe.461

[7] Mishra HK and Igarashi A (2012) Experimental and analytical study of scrap tire rubber pad for seismic isolation, International Journal of Civil, Environmental, Structural, Construction and Architectural Engineering, 6(2), 107-113.

[8] Mishra HK, Igarashi A, Matsushima H, Furukawa A (2012) Experimental and analytical study of unbonded and bonded scrap tire rubber pad as

base isolation device, 15th World Conference on Earthquake Engineering, Lisbon, Portugal.

[9] Mishra HK, Igarashi A, Matsushima H (2013) Finite element analysis and experimental verification of the scrap tire rubber pad isolator, Bulletin of Earthquake Engineering, 11, 687-707. https://doi.org/10.1007/s10518-012-9393-4

[10] Mishra HK, Igarashi A, Ji D, Matsushima H (2014) Pseudo-dynamic testing for seismic performance assessment of buildings with seismic isolation system using scrap tire rubber pad isolators, Journal of Civil Engineering and Architecture, 8(1), 73-88.

[11] Nakai T, Kurino H, Yaguchi T, Kano N (2019) Control effect of large tuned mass damper used for seismic retrofitting of existing high-rise building, Japan Architectural Review, 2(3), 269-286. https://doi.org/10.1002/2475-8876.12100

[12] Park J, Shirai K, Kikuchi M (2020) A seismic mass damper using scrap tire pads: experiment on mechanical property and analysis of control effect. The 17th World Conference on Earthquake Engineering, Sendai, Japan.

[13] Park J, Shirai K, Kikuchi M (2022) A seismic mass damper system using scrap tire pads: Loading tests on mechanical properties and numerical assessment of the response control effects, Soil Dynamics and Earthquake Engineering, vol. 157, 107257. https://doi.org/10.1016/j.soildyn.2022.107257

[14] Reyna R, Muñoz A, Zavala C, Diaz M (2018) Prototype of low cost seismic isolator using recycled tire sheets, 16th European Conference on Earthquake Engineering, Thessaloniki, Greece, 1-10.

[15] Sadek F, Mohraz B, Taylor AW, Chung RM (1997) A method of estimating the parameters of tuned mass dampers for seismic applications, Earthquake Engineering and Structural Dynamics, 26(6), 617-635. https://doi.org/10.1002/(SICI)1096-9845(199706)26:6<617::AID-EQE664>3.0.CO;2-Z

[16] Shinba R, Fujii D (2003) Housing quake-free system using waste tires, Summaries of Technical Papers of Annual Meeting, Architectural Institute of Japan, C-1, 135-136. (in Japanese)
[17] Shinba R, Fujii D (2004) Housing quake-free system using waste tires part 2 stiffness and response analysis of using waste tires, Summaries of Technical Papers of Annual Meeting, Architectural Institute of Japan, C-1, 435-436. (in Japanese)
[18] Shirai K, Park J (2020) Use of scrap tire pads in vibration control system for seismic response reduction of buildings, Bulletin of Earthquake Engineering, 18(5), 2497–2521. https://doi.org/10.1007/s10518-020-00787-2
[19] Turer A, Özden B (2008) Seismic base isolation using low-cost scrap tire pads (STP), Materials and Structures, 41, 891-908. https://doi.org/10.1617/s11527-007-9292-3
[20] Ueda Y, Ohba S (2005) Vibration tests of simple base-isolated foundation, Summaries of Technical Papers of Annual Meeting, Architectural Institute of Japan, C-1, 845-846. (in Japanese)
[21] Wang W, Hua X, Chen Z, Wang X, Song G (2019) Modeling, simulation, and validation of a pendulum-pounding tuned mass damper for vibration control, Structural Control and Health Monitoring, 26(4), e2326. https://doi.org/10.1002/stc.2326

Chapter II

Overview of seismic mass damper system using STP

The contents of this Chapter II have been published in the following paper.

Shirai K, Park J, "Use of scrap tire pads in vibration control system for seismic response reduction of buildings", Bulletin of Earthquake Engineering, 18(5), 2497–2521, 2020.

Overview of seismic mass damper system using STP

1. Introduction

The present study proposes a seismic mass damper (SMD) system for building structures using scrap tire pads (STPs) made from used tires. This proposed system aims to realize a high damping effect while adopting materials with high availability, economic efficiency, and reduced environmental burden. STPs are expected to have mechanical properties suitable for using them in the vibration control story of a seismic tuned mass damper (TMD) system. These properties include relatively high horizontal stiffness, sufficient horizontal deformability, sufficient vertical load-bearing capacity, and the possibility to omit the installation of additional energy dissipation devices.

2 Proposed Seismic Protection System Using Scrap Tire Pads

2.1 Concept of proposed system

Figure 2.1 shows a conceptual diagram of a STP manufactured by cutting up the treads (i.e., the side that directly contacts the road) of radial tires, which are typical tires for passenger cars. Each tire is divided such that the shapes and sizes of the obtained rubber pads are rectangular with approximately 100-mm width and 200-mm length. Roughly 7–12 rubber pads can be produced from one typical tire. Each rubber pad is laminated in a stack and bonded to adjacent pads.

By constructing a vibration control story using STPs at the top of the main frame of a building structure as shown in Figure 2.2, it is expected that the STPs act as vertical bearings against the weight of the additional mass and as horizontal springs with energy dissipation abilities during an earthquake.

2.2 Advantages

The proposed earthquake protection system is expected to have the following advantages:

- Seismic response reduction effect

By incorporating the proposed vibration control system, peak response, such as absolute acceleration of building structures under earthquakes, would be mitigated due to mass damper effects. This leads to a reduction of human injuries and damage to structural members, non-structural members, furniture, and equipment during strong earthquakes.

- Low impact to the environment

The proposed system would contribute to a reduced environmental burden by using waste materials. For example, in Japan almost 100 million waste tires (corresponding to around 1,000 kt) were generated each year from 2013 to 2017 inclusive (Japan Automobile Tyre Manufacturers Association). Effective reuse of such waste materials is an important social issue.

- Wide availability

The proposed system can be installed in buildings located in developing countries as well as developed countries. Because the main material of a STP is waste tires from common automobiles, it is easily obtained all around the world. Moreover, the process of making STPs from used tires and assembling them for the proposed system requires no special manufacturing techniques.

- Low cost

Because the STP is a recycled material, the proposed system can be constructed at low cost. Furthermore, STPs have a moderate damping performance even when they are incorporated alone, without adding other

energy damping devices (Turer and Özden 2008; Igarashi et al. 2013; Mishra et al. 2013). This further reduces the cost.

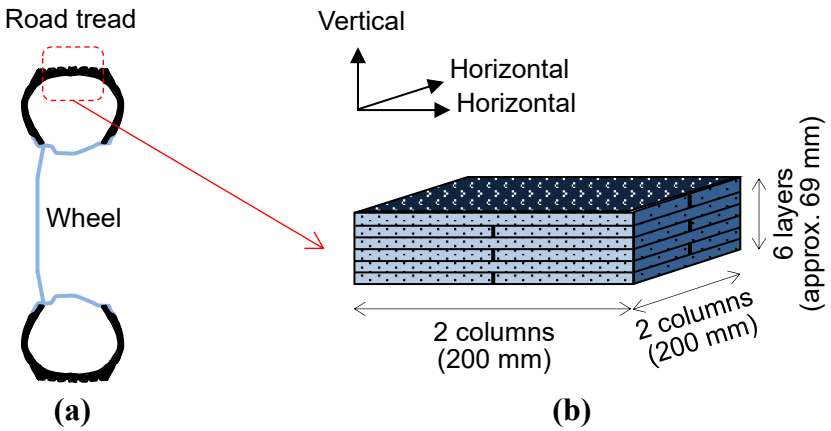

Figure 2.1 Conceptual diagrams of scrap tire pads: (a) sectional view of automobile tire; and (b) cabinet projection drawing of scrap tire pads unit

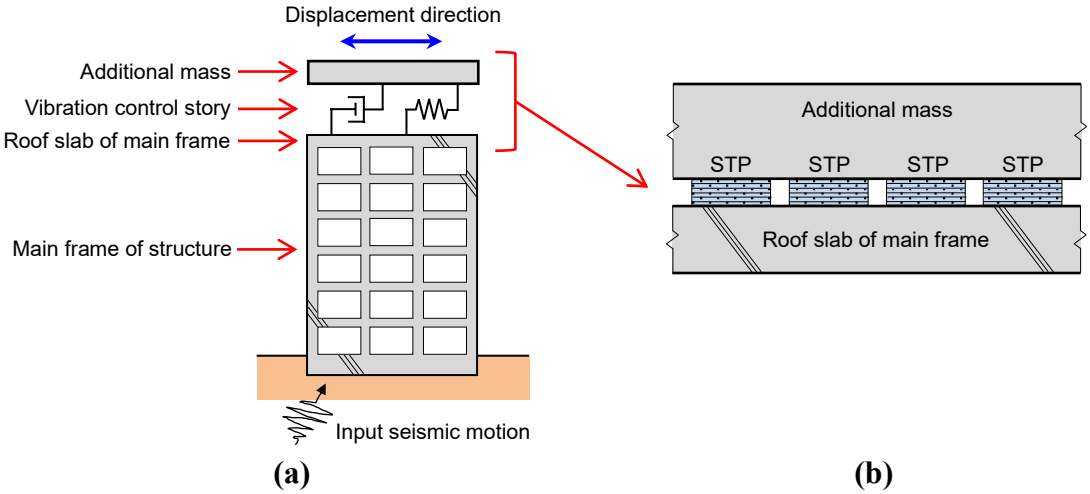

Figure 2.2 Conceptual diagram of a building structure incorporating proposed seismic vibration control system using scrap tire pads: (a) elevation view of whole system; and (b) enlarged view of vibration control story

3. Simple estimation of tire quantity for application to a building

To assess the feasibility of application of the proposed vibration control system, a simple estimation of necessary tire quantity for applying the proposed system to a building was conducted.

The proposed system should have as large a mass ratio as possible (i.e., the ratio of the mass of the vibration control system to that of the main structure) to improve the mass damper effect and its robustness. In this estimation, the mass ratio was assumed to be 5% or 10%. For example, by using other waste materials, such as concrete or asphalt debris, it might be possible to construct the mass body of a vibration control system having a mass ratio of around 0.05 or 0.1, without impairing economic rationality.

Table 2.1 gives the result of the estimation of the number of STP units and used tires needed to implement the proposed vibration control system in a fictional eight-story building. This building was assumed to have a regular plan and continuous stiffness distribution and its first vibration mode was supposed to be predominant. First, the main structure was simplified to a single-degree-of-freedom (SDOF) system, whose natural period was 0.48 s, and the mass of the first node was given as 8,000 t and the horizontal stiffness of the first story was obtained to be 1,371 MN/m. This mass of the first node of the SDOF system corresponded the effective (or equivalent) mass for the first vibration mode of the assumed eight-story building. The total horizontal stiffness of the vibration control story, whose mass ratio was 5% or 10%, was given using the optimal tuning design formula based on the fixed-point theory (Den Hartog 1956) of a two-degree-of-freedom (2DOF) system. In this model, the mass ratio is defined as the ratio of the mass of the second story to that of the first story. Then, the quantity of STP units and corresponding number of tires were obtained based on the STP stiffness data reported by a previous study (Igarashi et al. 2013). This estimation result

showed that the proposed system is expected to use a reasonable and realistic quantity of used tires. More information for calculating the required number of the STP units on building models are also explained in Chapters IV and V.

For allowing multiple STP units (such as 111 or 202 units in Table 2.1) to function in parallel for the horizontal direction, the whole height (total thickness) of each STP unit should be approximately equal when producing the STP units; and it is desirable that a rigid floor assumption in the horizontal direction should be applicable for the slab of the main frame where the mass damper system is installed.

Table 2.1 Estimation of quantity of scrap tire pads needed for proposed vibration control system when applied to a building with 2DOF model

Property	Value	
	Mass ratio 5%	Mass ratio 10%
Mass of main structure	8,000 t	
Natural period of main structure	0.48 s	
Lateral stiffness of main structure	1,371 MN/m	
Mass of vibration control system	400 t	800 t
Natural period of vibration control system *	0.504 s	0.528 s
Lateral stiffness of vibration control story	62.2 MN/m	113.3 MN/m
Plan size of each STP unit	200 mm × 200 mm	
Number of layers in each STP unit	6	
Horizontal stiffness of each STP unit	0.56 MN/m	
Number of STP units needed	111	202
Approximate number of used tires needed	111–190	202–346

* Calculated for vibration control system alone

4. Conclusions

A seismic vibration control system for building structures using STPs made from used tires was proposed. In addition to the earthquake response reduction effect, the proposed system has advantages in terms of low environmental impact, wide raw material availability, and low cost due to recycling of used tires as raw material.

References

[1] Den Hartog JP (1956) Mechanical vibrations (4th ed.), McGraw-Hill, New York.

[2] Igarashi A, Matsushima H, Mishra HK (2013) Investigation of material properties and shear deformation capacity of scrap tire rubber pad isolators, Journal of Japan Society of Civil Engineers, A1, 69(4), 958-964. (in Japanese) https://doi.org/10.2208/jscejseee.69.I_958

[3] Japan Automobile Tyre Manufacturers Association. (in Japanese) (Access date: July 30, 2019) http://www.jatma.or.jp/environment/report01.html

[4] Mishra HK, Igarashi A, Matsushima H (2013) Finite element analysis and experimental verification of the scrap tire rubber pad isolator, Bulletin of Earthquake Engineering, 11, 687-707. https://doi.org/10.1007/s10518-012-9393-4

[5] Shirai K, Park J (2020) Use of scrap tire pads in vibration control system for seismic response reduction of buildings, Bulletin of Earthquake Engineering, 18(5), 2497–2521. https://doi.org/10.1007/s10518-020-00787-2

[6] Turer A, Özden B (2008) Seismic base isolation using low-cost scrap tire pads (STP), Materials and Structures, 41, 891-908. https://doi.org/10.1617/s11527-007-9292-3

Chapter III

Experimental investigation on the mechanical characteristics of scrap tire pad (STP) specimens

The contents of this Chapter III have been published in the following paper.

Park J, Shirai K, Kikuchi M, "A seismic mass damper system using scrap tire pads: Loading tests on mechanical properties and numerical assessment of the response control effects", Soil Dynamics and Earthquake Engineering, vol. 157, 107257, 2022.

Experimental investigation on the mechanical characteristics of scrap tire pad (STP) specimens

1. Introduction

The present study aimed to understand the mechanical behavior of scrap tire pad (STP) units. The results of dynamic loading tests using four STP unit specimens, which were made of radial tires of different tire statuses (used or new) and manufacturers, are presented. In the tests, horizontal shear loading under a constant surface pressure was applied as well as vertical compression loading. In addition, the present paper is a significant revision of a previous study (Park et al. 2020) involving the addition of new experimental results.

2. Description of SMD system using STPs

Figure 3.1 depicts conceptual diagrams of the seismic mass damper (SMD) system using the STPs considered in the present study (Shirai and Park. 2020). An STP unit considered is produced by cutting up the tread portions of typical radial tires for passenger automobiles, as shown in Figure 3.1(a). Each rubber pad is divided from a whole tire to be a rectangular shape (e.g., 100 mm in width and 200 mm in length) and is then stacked (e.g., six layers) and bonded such that a single STP unit is created, as shown in Figure 3.1(b). An adequate number of STP units are placed at the mass damper story, i.e., between the roof of the superstructure of a building and an additional mass, as shown in Figure 3.1(c) and (d). The STP units are expected to act as not only a bearing (i.e., support the weight of the additional mass in the vertical direction) but also a horizontal spring and a damping element (i.e., a restoring force element and an energy dissipator). Thus, a vibration control system using STPs will work as a mass damper during an earthquake event (Figure 3.1(c)). For the mass damper story, the lower slab (i.e., the roof of the superstructure) under the STP units and the upper slab of the additional mass above the STP units (Figure 3.1(d)) were assumed to be constructed by reinforced concrete. The height of the STP units should be approximately the same. Two possible methods can be considered for fixing the SPT units to the lower and upper slabs: a method of fixing the STP units to the lower and upper slabs by adhesion; and a non-adhesion method that may involve slippage and rollover deformation between the STP units and slabs. In the case when the STP units undergo a large response deformation, the seismic response may change depending on the fixing method of the STP units.

The expected advantages of the SMD system using STPs are as follows: (i) seismic response reduction effects, (ii) low impact to the environment, (iii) wide availability of tires as a raw material, and (iv) low-cost. As for (ii), waste tires numbering around 86–96 million (approximately 0.9–1.0 Mt)

were generated in Japan each year from 2018 to 2020 (Japan Automobile Tyre Manufacturers Association). The SMD system using STPs is expected to reduce environmental impact by using used materials. Regarding (iii), since STPs are available globally and the production process of STPs requires no special production technologies, the SMD system can be applied to structures in both developing and developed countries. In addition, in the previous study by Shirai and Park (2020), the required tire quantity was estimated for constructing the SMD system using STPs in a building.

The proposed SMD system uses the principle of tuned mass dampers (TMDs) and is characterized by exerting damping performance owing to the inertial mass effect of the additional mass. On the other hand, base isolation systems have the characteristics of lengthening the period of the structure, decreasing the transmission of short-period component of input motions, and concentrating the deformation and energy absorption in the isolation story. Laminated rubber bearings with internal steel plates used for base-isolated buildings may be required to bear a surface pressure of 10–15 MPa or more. Because of the limitation of the vertical load carrying capacity, use of the STPs without internal steel plates as a bearing may not be suitable for the base-isolated buildings. If the superstructure is the same, compared to the weight of the superstructure in a base isolation building, the supporting weight by the STP units in the mass damper story of the SMD system is relatively small. Therefore, even the STPs without internal steel plates reinforcement can be applied as a bearing to the mass damper story of the SMD system. In addition, since the vertical stiffness of the STP units is lower than that of laminated rubber bearings with internal steel plates, there is a concern that the rocking response of the superstructure may increase if the STP units are installed in the isolation story of a base-isolated high-rise building. On the other hand, in the case that the STPs are applied to the mass damper story of the SMD system, the influence of the rocking response due to the vertical stiffness of the STP units is considered to be small.

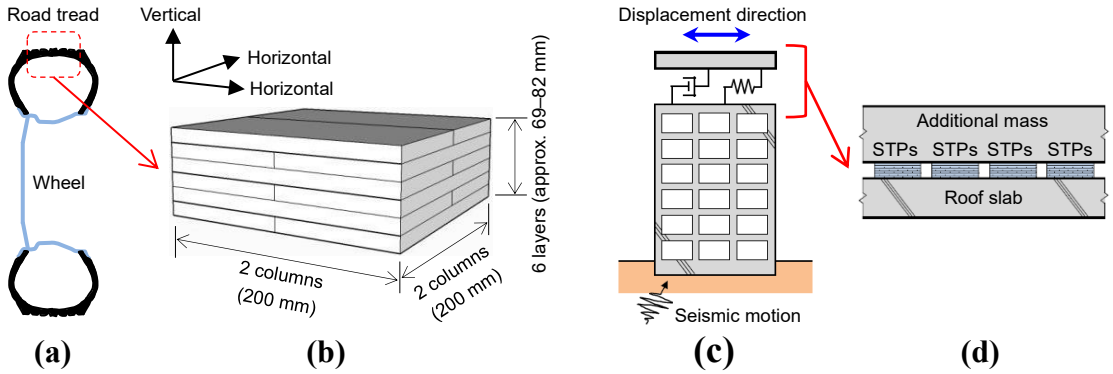

Figure 3.1 Conceptual diagrams of scrap tire pads (STPs) and the seismic mass damper (SMD) system: (a) sectional view of a radial tire for passenger cars; (b) single STP unit; (c) elevated view of the entire system; and (d) enlarged view of the mass damper story

3. Experimental methods

3.1 Description of test specimens and parameters

Dynamic loading tests were performed in the present study to grasp the mechanical characteristics of STP unit specimens with different tire statuses and manufacturers. A horizontal loading test under constant surface pressure was conducted as well as a vertical compression loading test. Based on the obtained results, the characteristics of the STPs of equivalent compression and shear stiffness and equivalent shear damping ratio were evaluated.

Four STP unit specimens, namely T1O, T1N, T2O, and T2N, were fabricated and used in the tests. Table 3.1 gives the specifications of each specimen. Radial tires for passenger cars were used as a raw material of the specimens. The tires used for specimens T1O and T1N were produced by one manufacturer (hereinafter referred as Manufacturer 1), whereas those for used for specimens T2O and T2N were produced by another manufacturer (hereinafter referred as Manufacturer 2). The status of the tires used for specimens T1N and T2N was new, whereas used tires with an estimated mileage of 5,000 to 8,000 km were used for specimens T1O and T2O. Regarding specimen T1O, the specimen details, fabrication process, test methods, and test results have been reported previously (Shirai and Park. 2020).

Table 3.1 Properties of the scrap tire pad (STP) unit specimens for the loading tests

Specimen	T1O	T1N	T2O	T2N
Type	195.65R 15			
Manufacturer	Manufacturer 1		Manufacturer 2	
Status	Used	New	Used	New
Estimated mileage	5,000–8,000 km	0	5,000–8,000 km	0
Planar configuration	200 mm × 200 mm (width 100 mm × length 200 mm × 2 columns)			
Number of layers	6			
Thickness	68.75 mm	75.5 mm	74.5 mm	81.75 mm

3.2 Preparation of test specimens

Figure 3.2 shows photographs of the production process of the specimens. Rubber pads were cut from the tread part of the tires into a rectangular shape (a width of approximately 100 mm and a length of approximately 200 mm). Each rubber pad had a thickness of roughly 11 to 14 mm and they were stacked using rubber glue such that each STP unit had six layers. The front and front sides and the back and back sides of the rubber pads became pairs and overlapped with each other such that the tread surface was placed at the top and bottom sides of the STP unit. The surface opposite the tire tread was polished with a sander before the adhesion in order to increase the bonding performance. After applying the rubber glue, the rubber pads were laminated and compressed with clamps in order to prevent warping. Figure 3.3 shows photographs of each specimen. The total thickness of the STP unit specimens made of used tires (i.e., T1O and T2O) became relatively low due to wear compared with the specimens made of new tires (i.e., T1N and T2N).

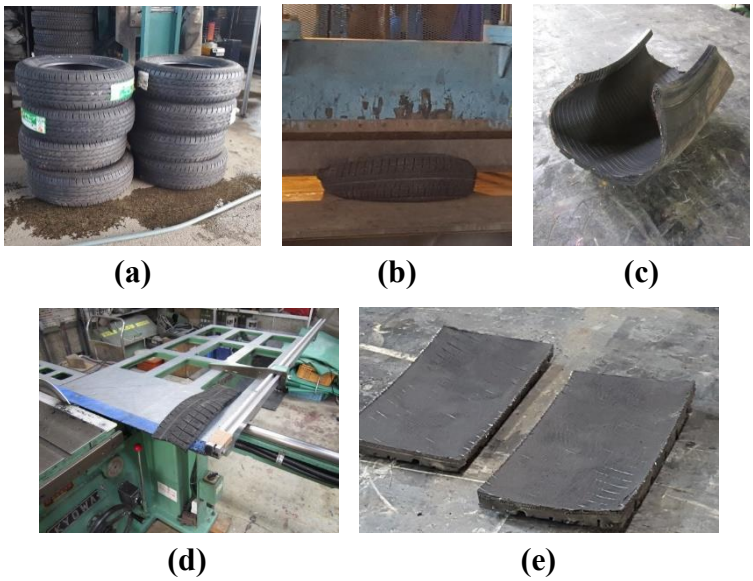

Figure 3.2 Process for producing STP unit specimens for the loading tests: (a) radial tires; (b) initial cutting by shear; (c) after initial cutting; (d) after additional cutting; and (e) before applying rubber cement

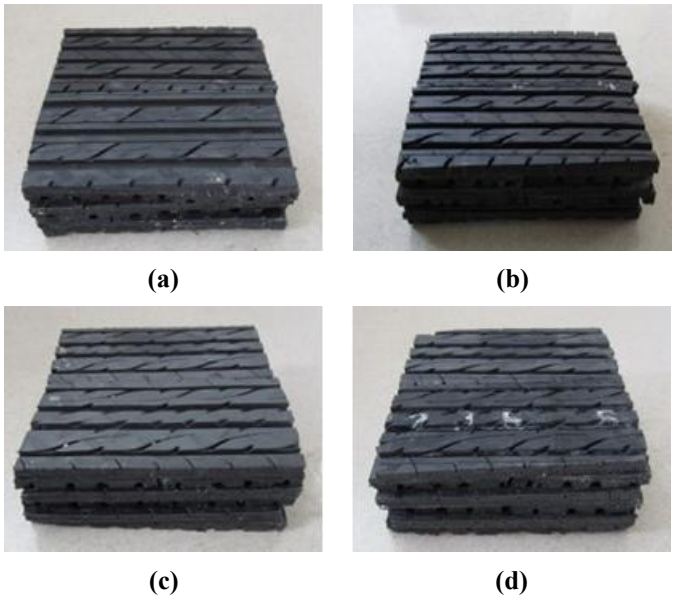

Figure 3.3 STP unit specimens for the loading tests: (a) T1O; (b) T1N; (c) T2O; and (d) T2N

3.3 Experimental program

The loading program for the tests is listed in Table 3.2. The same loading program was adopted for each specimen. The loading program consisted of 23 loading runs with various loading conditions, including the surface pressure, loading frequency, loading displacement amplitude, and cycle number. Vertical loading was conducted in Run 1 in order to obtain the compression stiffness characteristics of STP units, whereas vertical loading was performed in Run 23 in order to verify that STP units can withstand a vertical pressure of up to 5.0 MPa. Runs 2–22 were horizontal sinusoidal loadings under constant vertical pressure in order to clarify the mechanical behavior of STP units in the shear direction.

Table 3.2 Loading test program for each specimen

Run	Vertical load [kN]	Vertical pressure [MPa]	Horizontal loading frequency [Hz]	Target horizontal loading amplitude [mm]	Number of cycles	Loading axis *
1	up to 40	up to 1.0	-	-	-	V
2	40	1.0	0.25	5	3	H+V
3	40	1.0	1.0	5	3	H+V
4	40	1.0	2.0	5	3	H+V
5	40	1.0	3.0	5	3	H+V
6	40	1.0	0.25	10	3	H+V
7	40	1.0	1.0	10	3	H+V
8	40	1.0	2.0	10	3	H+V
9	40	1.0	3.0	10	3	H+V
10	40	1.0	0.25	20	3	H+V
11	40	1.0	1.0	20	3	H+V
12	40	1.0	2.0	20	3	H+V
13	20	0.5	0.25	5	3	H+V
14	20	0.5	0.25	10	3	H+V
15	20	0.5	0.25	20	3	H+V
16	80	2.0	0.25	5	3	H+V
17	80	2.0	0.25	10	3	H+V
18	80	2.0	0.25	20	3	H+V
19	40	1.0	0.25	20	30	H+V
20	40	1.0	0.25	40	3	H+V
21	40	1.0	0.25	60	3	H+V
22	40	1.0	0.25	80	3	H+V
23	up to 200	up to 5.0	-	-	-	V

* V = vertical uniaxial loading, H+V = horizontal loading under constant vertical pressure

3.4 Test setup and instrumentation

The tests were conducted using a biaxial loading machine. A pair of checker plates were installed in the loading machine, and each STP unit was placed and sandwiched between the bottom and upper checker plates without bonding.

4. Experimental results and discussion

4.1 Vertical characteristics

Vertical loadings with three cycles were conducted in Run 1 and Run 23, in which the surface pressure was increased up to 1.0 and 5.0 MPa, respectively, for each STP unit specimen. Figure 3.4 shows the load-displacement relationship in the vertical direction (at the third cycle) obtained from Run 1 for each specimen. The vertical equivalent stiffness, K_v, and the vertical equivalent Young's modulus, E_v, for each specimen was calculated from the test results as follows:

$$K_v = (F_1 - F_2)/(\Delta_1 - \Delta_2) \quad (1)$$

$$E_v = (K_v\, t)/A \quad (2)$$

where F_2 and F_1 are the minimum and maximum vertical loads, respectively, and Δ_2 and Δ_1 are the displacements corresponding to F_2 and F_1, respectively, obtained from the test results (at the third cycle). In addition, t is the overall thickness, and A is the horizontal area of each STP unit specimen.

Table 3.3 gives the values of each variable in Eqs. (1) and (2) obtained from Run 1 for each specimen. The vertical equivalent stiffness of specimens T1O, T1N, T2O, and T2N in Run 1 was calculated to be K_v = 8.40, 6.50, 9.08, and 5.57 kN/mm, respectively. In addition, the corresponding Young's modulus was calculated to be E_v =14.43, 12.28, 16.90, and 11.39 N/mm2, respectively. It can be seen from the results that Young's modulus of the specimens made of used tires (T1O and T2O) was higher compared with those made of new tires (T1N and T2N).

Figure 3.5 depicts the vertical load–displacement relationships (at the third cycle) obtained from Run 23 for each specimen. Even under a vertical load of up to roughly 200 kN, no apparent damage was observed for any of the STP unit specimens. The results indicate that STP units were able to withstand a vertical compressive pressure of at least 5.0 MPa without failure.

A vertical pressure capacity of 5.0 MPa of the STP unit specimens may be insufficient for use as a bearing for usual base-isolated building structures but can be considered to be adequate for use in an SMD system the mass ratio of which is 10% or less.

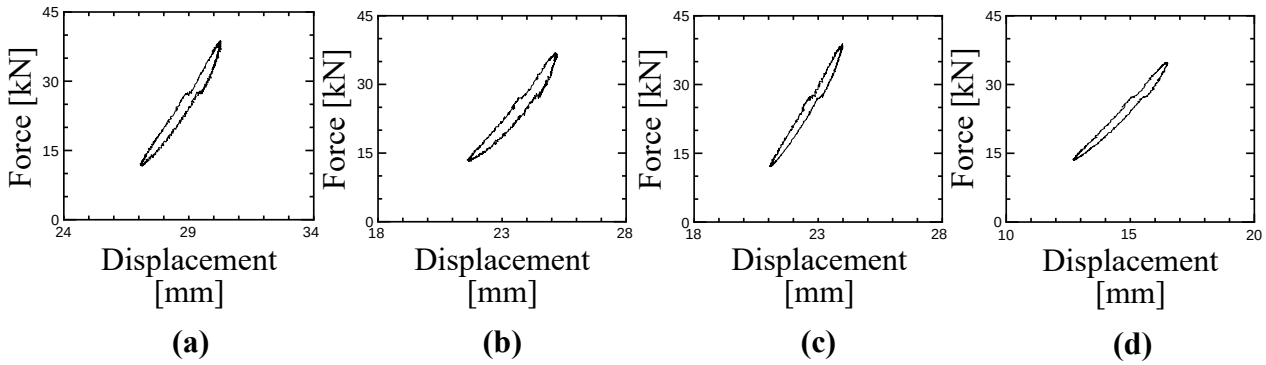

Figure 3.4 Vertical load–displacement curves obtained from Run 1 (surface pressure up to 1.0 MPa): (a) T1O; (b) T1N; (c) T2O; and (d) T2N

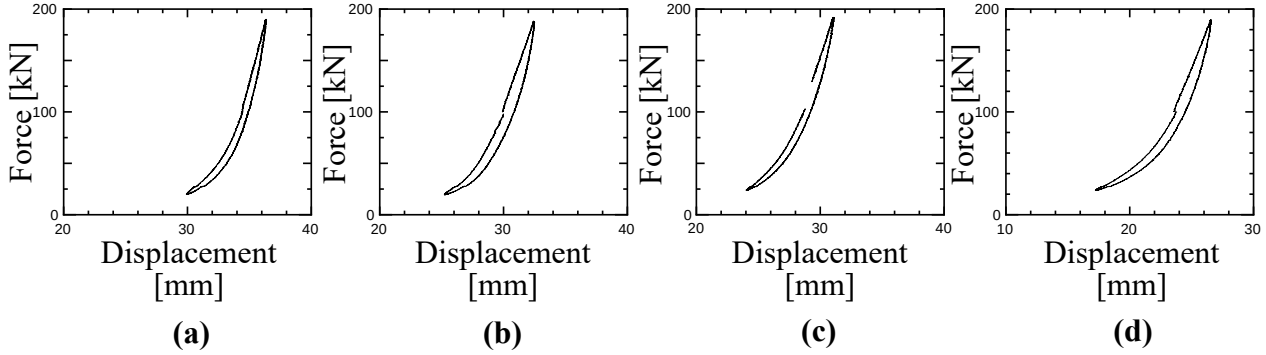

Figure 3.5 Vertical load–displacement curves obtained from Run 23 (surface pressure up to 5.0 MPa): (a) T1O; (b) T1N; (c) T2O; and (d) T2N

Table 3.3 Equivalent stiffness and Young's modulus in the vertical (compressive) direction for each specimen

Symbol	Unit	T1O	T1N	T2O	T2N
F_1	kN	38.85	36.96	38.94	34.88
F_2	kN	11.58	13.16	12.05	13.50
Δ_1	mm	30.30	25.24	24.01	16.52
Δ_2	mm	27.05	21.58	21.05	12.68
K_v	kN/mm	8.40	6.50	9.08	5.57
t	mm	68.75	75.5	74.5	81.75
A	mm^2	40,000	40,000	40,000	40,000
E_v	N/mm^2	14.43	12.28	16.90	11.39

4.2 Horizontal characteristics

4.2.1 Response waveforms in time history

The obtained response in the horizontal direction from the horizontal loadings is shown in Figures 3.6–3.13. Figures 3.6 and 3.7 show the horizontal response waveforms for the time history displacements and forces, respectively, under a pressure of 1.0 MPa with a loading frequency of 0.25 Hz obtained from Run 2 (loading displacement 5 mm), Run 6 (10 mm), and Run 10 (20 mm) for specimen T1N. These results indicate that the waveforms pictured approximately sinusoidal and stable wave shapes. Figure 3.12(b) depicts the time history waveforms of the horizontal force of Run 19 (30 cycles, surface pressure 1.0 MPa, loading displacement 20 mm, loading frequency 0.25 Hz) for specimen T2O. From Figure 3.12(b), the response force fluctuation was not large during the 30-cycle repetitive loading. No damage or breakage was observed in the STP unit specimens during or after the 30-cycle loadings.

4.2.2 Hysteresis loops

Figures 3.8–3.11, 3.12(a), and 3.13 illustrate the load–displacement relationships in the horizontal direction. Overall, in the horizontal loading tests, each STP unit specimen demonstrated a roughly similar stable response behavior and a thick oval or spindle-shaped hysteresis loop. This indicates that STP units have a moderate damping performance, which is consistent with findings reported on past research (Turer and Özden. 2008; Mishra et al. 2013; Igarashi et al. 2013). Figures 3.8 and 3.9 show the obtained hysteresis loops under different loading frequencies for displacement amplitudes of 5 and 10 mm, respectively, at a vertical pressure of 1.0 MPa for specimen T2O. The results indicate that, as the loading frequency increased, the area of the hysteretic loops (i.e., consumed energy amount) tended to increase. Figure 3.10 compares the hysteresis loops of all four specimens for Run 12 (vertical pressure 1.0 MPa, loading displacement 20 mm, loading frequency 2.0 Hz). As shown in Figure 3.10, the equivalent stiffness of the horizontal hysteresis loops for the specimens made of used tires (T1O and T2O) was higher than that for new tires (T1N and T2N). Figure 3.11 shows the hysteresis loops under vertical pressures of 0.5, 1.0, and 2.0 MPa (loading displacement 20 mm, loading frequency 0.25 Hz) for specimen T2N. This indicates that the equivalent stiffness of the hysteresis loops slightly increased as the surface pressure increased. Figure 3.12(a) shows the loops obtained from Run 19 (30-cycle repetitive loading, vertical pressure 1.0 MPa, loading displacement 20 mm, loading frequency 0.25 Hz) for specimen T2O. From Figure 3.12(a), a stable loop was observed during the 30-cycle loading. Figure 3.13 shows the loops under loading displacements of 40, 60, and 80 mm (vertical pressure 1.0 MPa, loading frequency 0.25 Hz) for specimen T2O. This showed that, as the loading amplitude increased, the area of the loops increased. Although all four specimens had a sliding motion around the negative-side peak deformation point at Run 22 (loading displacement 80 mm), no damage or breakage was

observed for any specimen during or after Run 22.

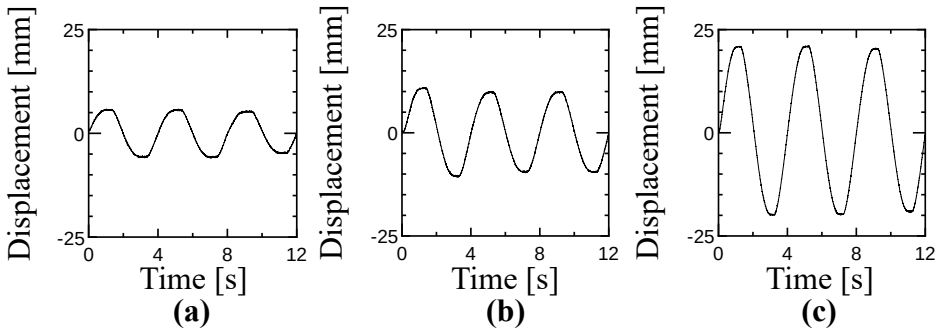

Figure 3.6 Time history displacement in the horizontal direction (T1N, loading frequency 0.25 Hz, surface pressure 1.0 MPa): (a) loading displacement of 5 mm (Run 2); (b) loading displacement of 10 mm (Run 6); and (c) loading displacement of 20 mm (Run 10)

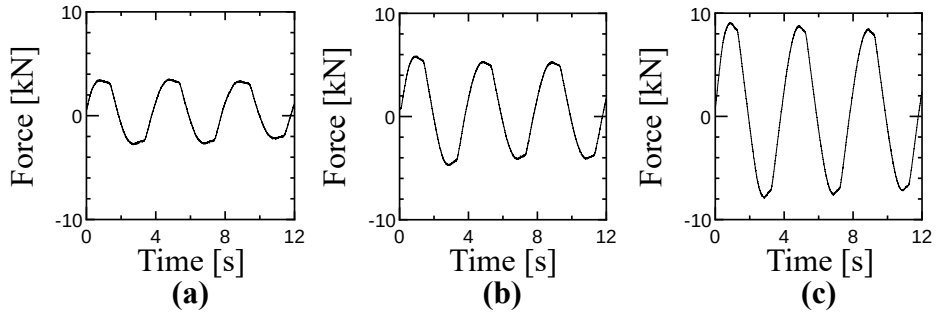

Figure 3.7 Time history shear force in the horizontal direction (T1N, loading frequency 0.25 Hz, surface pressure 1.0 MPa): (a) loading displacement of 5 mm (Run 2); (b) loading displacement of 10 mm (Run 6); and (c) loading displacement of 20 mm (Run 10)

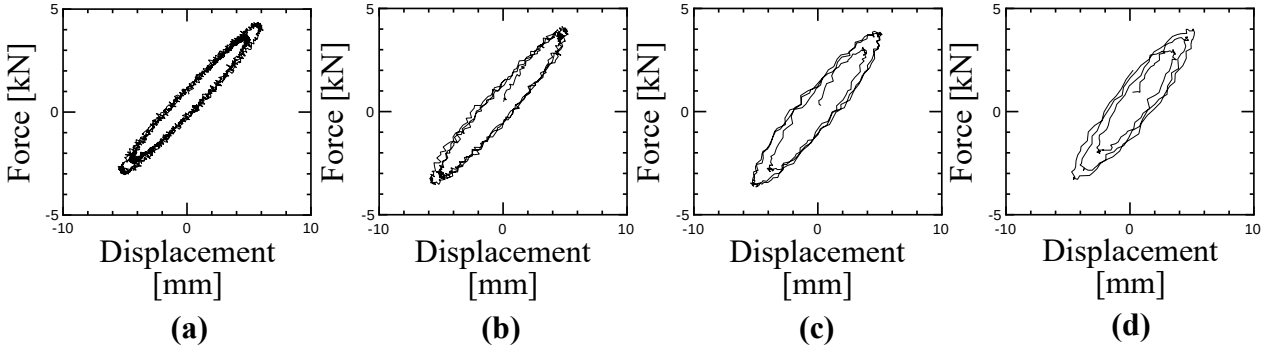

Figure 3.8 Horizontal load–displacement hysteresis loops under different loading frequencies (T2O, loading displacement 5 mm, surface pressure 1.0 MPa): (a) loading frequency of 0.25 Hz (Run 2); (b) loading frequency of 1.0 Hz (Run 3); (c) loading frequency of 2.0 Hz (Run 4); and (d) loading frequency of 3.0 Hz (Run 5)

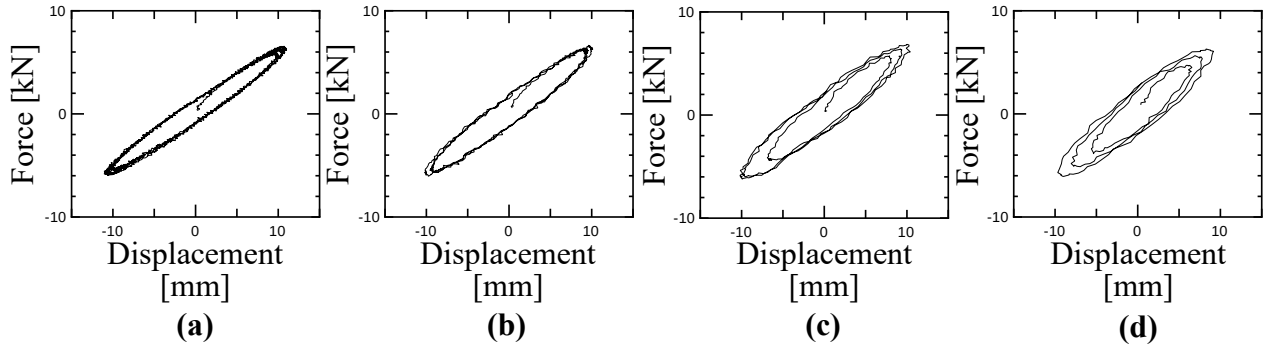

Figure 3.9 Horizontal load–displacement hysteresis loops under different loading frequencies (T2O, loading displacement 10 mm, surface pressure 1.0 MPa): (a) loading frequency of 0.25 Hz (Run 6); (b) loading frequency of 1.0 Hz (Run 7); (c) loading frequency of 2.0 Hz (Run 8); and (d) loading frequency of 3.0 Hz (Run 9)

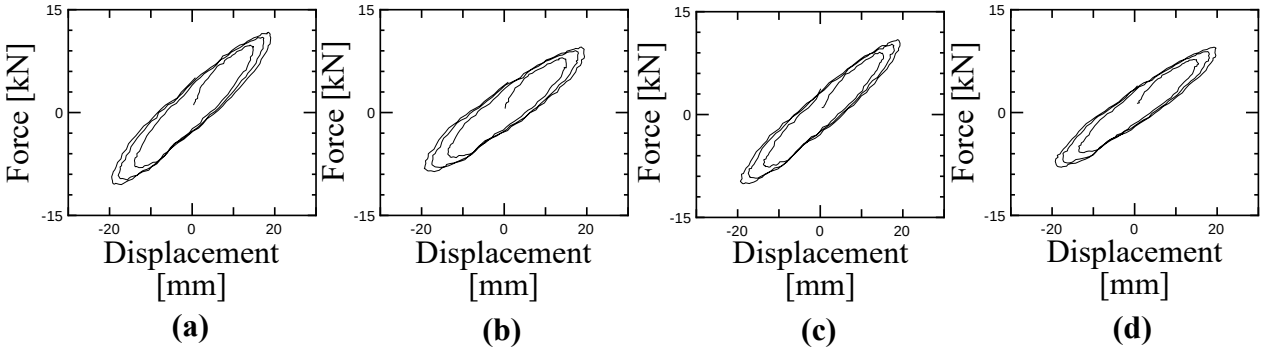

Figure 3.10 Horizontal load–displacement hysteresis loops for each specimen (Run 12, loading displacement 20 mm, surface pressure 1.0 MPa, loading frequency 2.0 Hz): (a) T1O; (b) T1N; (c) T2O; and (d) T2N

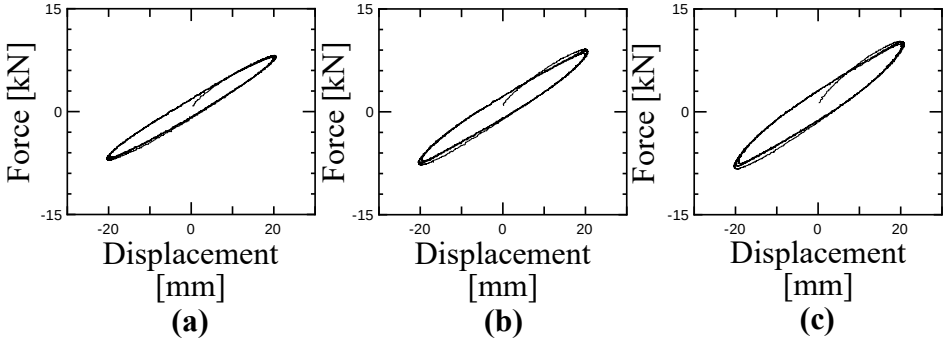

Figure 3.11 Horizontal load–displacement hysteresis loops under different vertical pressures (T2N, loading frequency 0.25 Hz, loading displacement 20 mm): (a) surface pressure of 0.5 MPa (Run 15); (b) surface pressure of 1.0 MPa (Run 10); and (c) surface pressure of 2.0 MPa (Run 18)

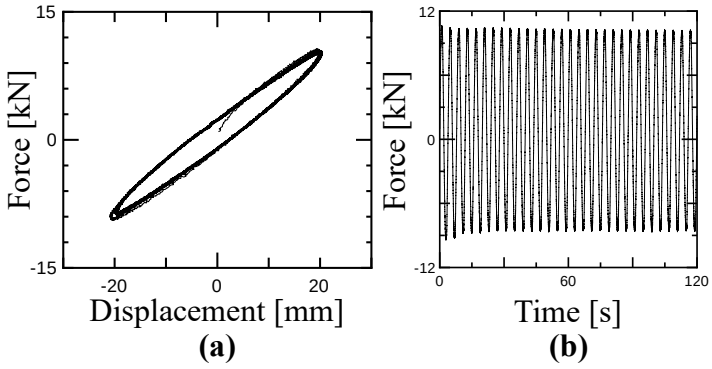

Figure 3.12 Response under 30-cycle loading (T2O, Run 19, loading frequency 0.25 Hz, loading displacement 20 mm, surface pressure 1.0 MPa): (a) hysteresis loop; and (b) time history shear force

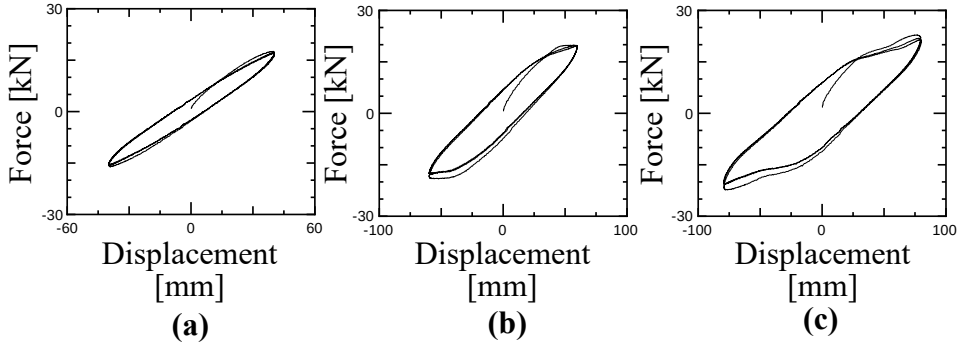

Figure 3.13 Horizontal hysteresis loops under different loading displacement amplitudes (T2O, loading frequency 0.25 Hz, surface pressure 1.0 MPa): (a) loading displacement of 40 mm (Run 20); (b) loading displacement of 60 mm (Run 21); and (c) loading displacement of 80 mm (Run 22)

4.2.3 Frequency dependence

The horizontal equivalent stiffness and damping factor were evaluated for each Run and for each STP unit specimen. The horizontal equivalent stiffness, Keq, and the horizontal equivalent viscous damping factor, h_{eq}, were calculated from the test results as follows:

$$K_{eq} = (Q_{max} - Q_{min})/(X_{max} - X_{min}) \quad (3)$$

$$h_{eq} = \Delta W/(4\,\pi\, W) = 2\,\Delta W/[\pi\, K_{eq}\,(X_{max} - X_{min})^2] \quad (4)$$

where Q_{min} and Q_{max} are the minimum and maximum forces, respectively, and X_{min} and X_{max} are the minimum and maximum displacements, respectively, in the horizontal direction for each cycle of the obtained hysteresis loops. Moreover, ΔW and W are the energy loss and the potential deformation energy of K_{eq}, respectively, in the horizontal direction for each cycle of the hysteresis loops. Hereinafter, for Runs 2–22 (except for Run 19), the values of K_{eq} and h_{eq} calculated at the third cycle of the three-cycle-loading were used.

Figures 3.14(a) and 3.14(b) plot the calculated equivalent stiffness K_{eq} and equivalent damping factor h_{eq}, respectively, against loading frequency for all specimens (loading displacement 10 mm, surface pressure 1.0 MPa). From Figure 3.14(a), for each specimen, as the loading frequency increased, the obtained K_{eq} gradually increased. However, the increasing rate of change gradually decreased. From Figure 3.14(b), as the loading frequency increased, the obtained value of h_{eq} increased for each specimen.

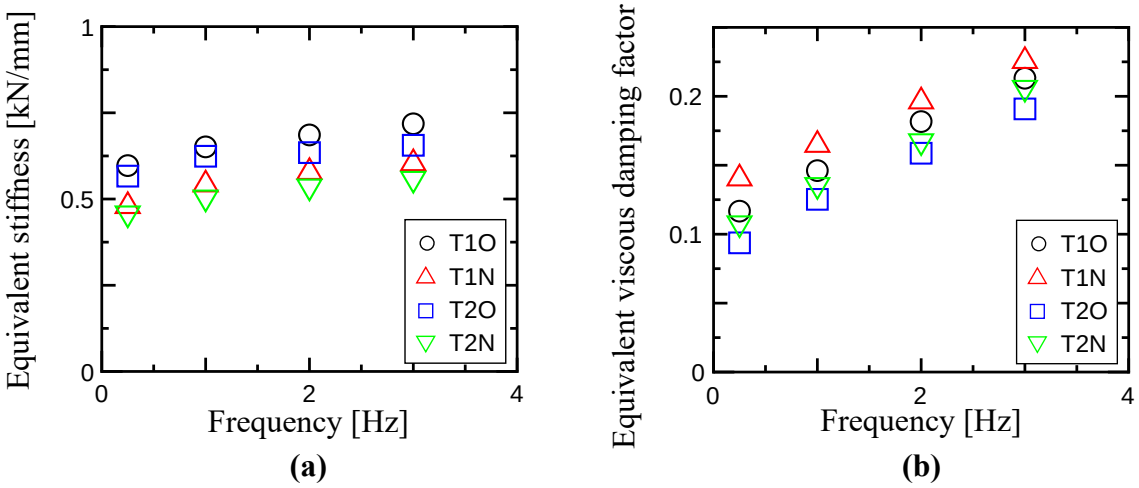

Figure 3.14 Frequency dependence of the equivalent stiffness and damping in the horizontal direction (displacement amplitude 10 mm, surface pressure 1.0 MPa): (a) equivalent stiffness; and (b) equivalent viscous damping factor

4.2.4 Surface pressure dependence

Figures 3.15(a) and 3.15(b) show the calculated K_{eq} and h_q, respectively, against surface pressure for all specimens (loading displacement 20 mm, loading frequency 0.25 Hz). From Figure 3.15(a), all specimens tended to increase their equivalent stiffness as the surface pressure increased. In addition, the obtained h_{eq} slightly increased with increasing surface pressure, except for specimen T2O (Figure 3.15(b)).

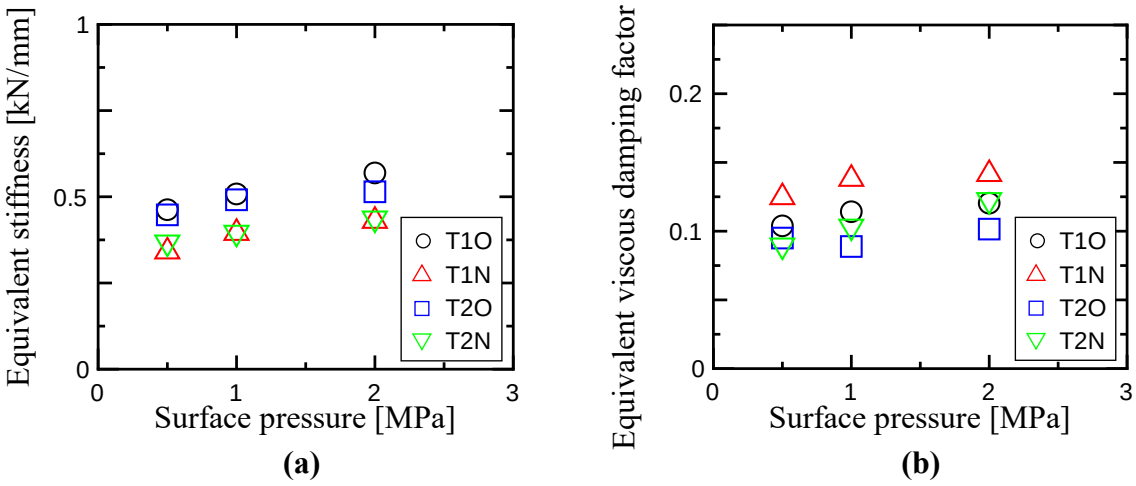

Figure 3.15 Surface pressure dependence of the equivalent stiffness and damping in the horizontal direction (loading frequency 0.25 Hz, displacement amplitude 20 mm): (a) equivalent stiffness; and (b) equivalent viscous damping factor

4.2.5 Amplitude dependence

Figures 3.16(a) and 3.16(b) plot K_{eq} and h_{eq}, respectively, against loading displacement amplitudes of 5 to 80 mm (surface pressure 1.0 MPa, loading frequency 0.25 Hz) for all specimens. The results of Figure 3.16(a) indicated that for each specimen, the greater the loading displacement amplitude, the lower the equivalent stiffness. From Figure 3.16(b), h_{eq} generally decreased as the loading displacement amplitude increased within the displacement range of around 40 mm. Beyond this displacement range, the equivalent damping factor began to increase as the loading amplitude increased, except for specimen T1N. This was likely due to the effect of a slippage behavior between the STP unit and checker plates that occurred around a displacement amplitude of roughly 60 mm or more.

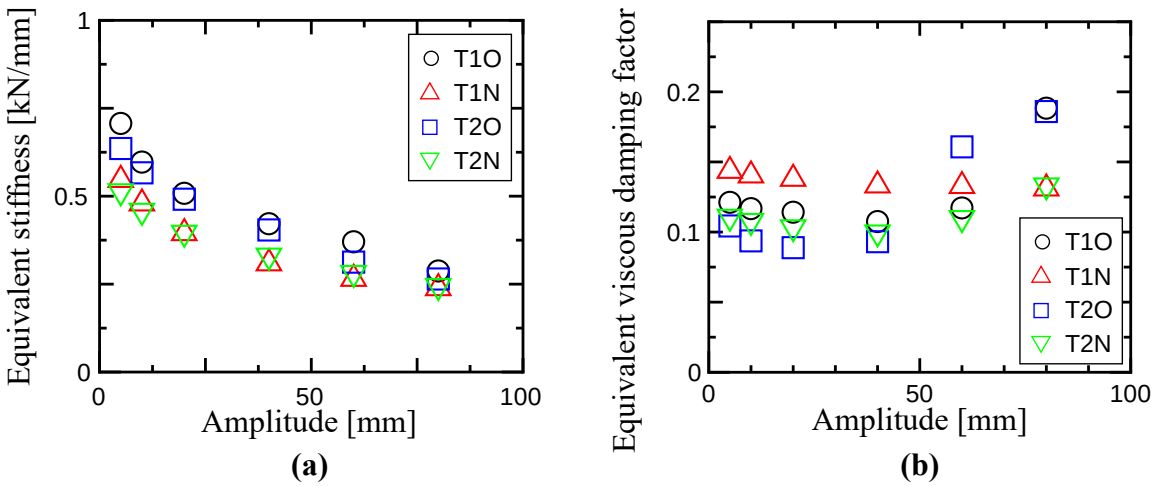

Figure 3.16 Amplitude dependence of the equivalent stiffness and damping in the horizontal direction (loading frequency 0.25 Hz, surface pressure 1.0 MPa): (a) equivalent stiffness; and (b) equivalent viscous damping factor

4.2.6 Repetitive loading dependence

Figures 3.17(a) and 3.17(b) show K_{eq} and h_{eq}, respectively, against the cycle number in 30-cycle loading of Run 19 (surface pressure 1.0 MPa, loading displacement 20 mm, loading frequency 0.25 Hz) for all specimens. From Figure 3.17(a), the equivalent stiffness changed slightly over the first five cycles, followed by almost no change in the subsequent cycles. In addition, the equivalent stiffness of specimens T1O, T1N, T2O, and T2N decreased 6.6%, 7.8%, 3.8%, and 4.7%, respectively, when comparing the last (i.e., 30-th) cycle to the first cycle. Moreover, from Figure 3.17(b), the equivalent damping factor demonstrated an almost constant value during the 30-cycle loading. The equivalent damping factors of specimens T1O, T1N, T2O, and T2N at the last cycle changed 0.7%, 2.4%, 2.1%, and 2.5%, respectively, as compared with the first cycle. These results indicate that the performance of the equivalent stiffness and damping factor was not significantly reduced by repetitive loadings. Moreover, it was externally observed that each STP unit specimen was neither broken nor damaged after the 30-cycle loading.

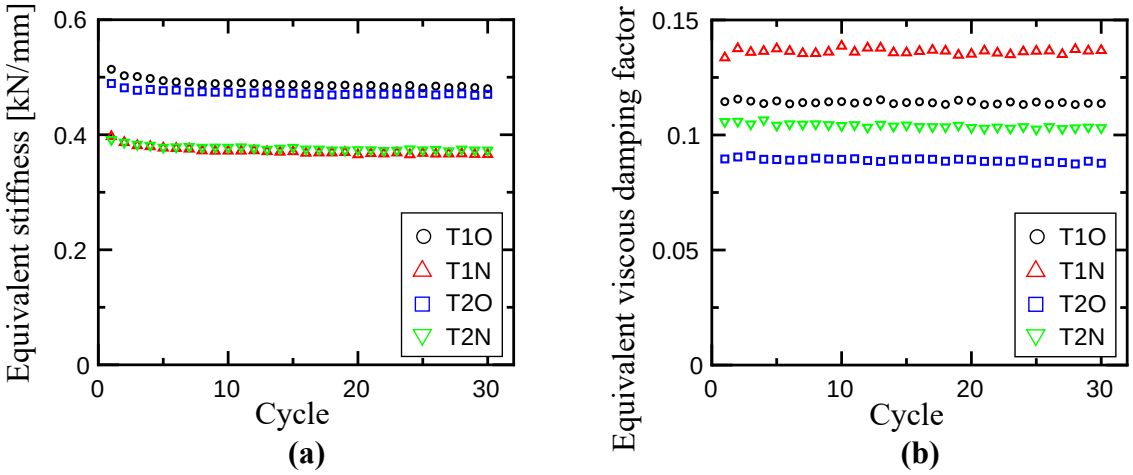

Figure 3.17 Cyclic loading dependence of the equivalent stiffness and damping in the horizontal direction (Run 19, loading frequency 0.25 Hz, displacement amplitude 20 mm, surface pressure 1.0 MPa): (a) equivalent stiffness; and (b) equivalent viscous damping factor

4.2.7 Effects of difference of tire status and manufacturer

From the test results shown in Figures 3.10 and 3.14–3.17, a basically similar tendency in the horizontal directional behavior was observed for all STP unit specimens, even when different tire statuses (new or used) and manufacturers (Manufacturer 1 or Manufacturer 2) were used for the specimens. Regarding the difference of tire status, Figures 3.14–3.17 show that the specimens made of used tires (T1O and T2O) tended to have a higher equivalent stiffness than those made of new tires (T1N and T2N). On the other hand, from Figures 3.14, 3.15, and 3.17, the equivalent damping factors of the specimens using the new tires (T1N and T2N) tended to be larger than those for the used tires (T1O and T2O). Regarding the difference of the tire manufacturer, there was a slight difference in equivalent stiffness between the specimens of Manufacturer 1 (T1O and T1N) and Manufacturer 2 (T2O and T2N) in Figure 3.14. However, no significant difference in equivalent stiffness between Manufacturer 1 and Manufacturer 2 was observed in Figure 3.15–3.17. In addition, Figures 3.14, 3.15, and 3.17 showed that the specimens made using Manufacturer 1 tires tended to have a larger equivalent damping factor than those made using Manufacturer 2 tires. In the present study, the used tires with an estimated mileage of 5,000–8,000 km were used for the specimens T1O and T2O, however, the degree of deterioration of the used tires due to other factors such as aging was not distinguished. In general, tire deterioration factors include not only wear due to service use related to mileage, but also aging and chemical factors such as due to UV and heat. Thus, the characteristics of the STPs can be affected and varied by a combination of these factors.

5. Conclusions

Loading test results using four six-layered STP unit specimens with different tire statuses and manufacturers were presented. The following conclusions were drawn.

1) In the vertical loading tests, all STP unit specimens were able to withstand a vertical compressive pressure of 5.0 MPa without failure. Also, Young's modulus E_v was evaluated to be 11.4–16.9 N/mm^2.

2) In the horizontal loading tests under a constant vertical pressure, each STP unit specimen demonstrated stable behavior and a thick hysteresis loop, indicating a moderate damping ability without the addition of other energy dissipators. The obtained horizontal equivalent stiffness and viscous damping factor were approximately 0.24–0.72 kN/mm and 0.09–0.23, respectively.

3) For each specimen, the horizontal equivalent stiffness gradually increased as the loading frequency increased, whereas the increasing rate of change gradually decreased. The horizontal equivalent damping factor increased as the loading frequency increased. The greater the loading displacement amplitude, the lower the equivalent stiffness. Moreover, no significant reduction in the equivalent stiffness and damping factor was observed under 30-cycle loadings.

4) A similar tendency in the horizontal behavior was observed for all specimens. The specimens made of used tires with an estimated mileage of 5,000–8,000 km tended to have a higher equivalent stiffness than those made of new tires, whereas the equivalent damping factor of the specimens using new tires tended to be larger than those using used tires. A slight difference in the equivalent stiffness between the specimens of Manufacturer 1 and Manufacturer 2 was observed.

Future research tasks include investigation on the effect of deterioration including aging to the characteristics variation of the STPs.

References

[1] Igarashi A, Matsushima H, Mishra HK (2013) Investigation of material properties and shear deformation capacity of scrap tire rubber pad isolators. Journal of Japan Society of Civil Engineers, A1, 69(4), 958-964. (in Japanese)
https://doi.org/10.2208/jscejseee.69.I_958

[2] Japan Automobile Tyre Manufacturers Association. (in Japanese) (Access date: November 12, 2021)
https://www.jatma.or.jp/environment_recycle/aboutscraptyres.html

[3] Mishra HK, Igarashi A, Matsushima H (2013) Finite element analysis and experimental verification of the scrap tire rubber pad isolator, Bulletin of Earthquake Engineering. 11, 687-707.
https://doi.org/10.1007/s10518-012-9393-4

[4] Park J, Shirai K, Kikuchi M (2020) A seismic mass damper using scrap tire pads: experiment on mechanical property and analysis of control effect. The 17th World Conference on Earthquake Engineering, Sendai, Japan.

[5] Park J, Shirai K, Kikuchi M (2022) A seismic mass damper system using scrap tire pads: Loading tests on mechanical properties and numerical assessment of the response control effects, Soil Dynamics and Earthquake Engineering, vol. 157, 107257.
https://doi.org/10.1016/j.soildyn.2022.107257

[6] Shirai K, Park J (2020) Use of scrap tire pads in vibration control system for seismic response reduction of buildings. Bulletin of Earthquake Engineering, 18(5), 2497–2521.
https://doi.org/10.1007/s10518-020-00787-2

[7] Turer A, Özden B (2008) Seismic base isolation using low-cost scrap tire pads (STP). Materials and Structures, 41, 891-908.
https://doi.org/10.1617/s11527-007-9292-3

Chapter IV

Numerical assessment of control effects for linear building structure models

The contents of this Chapter IV have been published in the following paper.

Shirai K, Park J, "Use of scrap tire pads in vibration control system for seismic response reduction of buildings", Bulletin of Earthquake Engineering, 18(5), 2497–2521, 2020.

Numerical assessment of control effects for linear building structure models

1. Introduction

In the present study, to assess the vibration control effect of the proposed system, earthquake response analysis under various earthquake motions was carried out using single-degree-of-freedom (SDOF) or two-degree-of-freedom (2DOF) models based on the mechanical properties obtained in the tests. The methods and results of the analysis are presented in this study. In addition, this study expands on previous reports (Shirai et al. 2015; 2017; Park et al. 2017) by presenting new analytical results and findings.

2. Analytical methods

2.1 Modeling of main structure

Eleven simplified building structure models with linear time-invariant characteristics were used for the analysis. The first one was a non-controlled model named Case N, which was a SDOF system without any vibration control techniques. The others were controlled models representing 2DOF systems incorporating the proposed seismic mass damper using scrap tire pad (STP). Cases M05A, M05B, M05C, M05D, and M05E employed a mass ratio of 5% and Cases M10A, M10B, M10C, M10D, and M10E employed a mass ratio of 10%. These mass ratios refer to the ratio of the mass of the second story (i.e., the vibration control system) to that of the first story (i.e., the main structure). The model properties of the first story for each analytical case and the second story for Cases M05A and M10A were the same as those used in Chapter II. The analytical models of the non-controlled and controlled systems are depicted in Figure 4.1. The properties of the models are given in Table 4.1. The property of the main structure (i.e., the mass and stiffness of the first story) was the same for each case. The main structure of each model was supposed as a building having a natural period for the first mode of 0.48 s.

2.2 Modeling of vibration control system

For controlled Case M05A, the additional mass of the vibration control story was set at the top of the main structure such that the mass ratio was 0.05. Six-layer STP units (plan of 200 mm × 200 mm) were placed in the vibration control story of the model. Based on the results obtained from the loading tests in Chapter III with a frequency of 2 Hz and amplitude of 20 mm, an equivalent stiffness $K_{eq,STP}$ of 0.56 MN/m and equivalent viscous damping factor $h_{eq,STP}$ of 0.17 were adopted for each STP unit.

Similar to the quantity estimation in Chapter II, the property of the total lateral stiffness of the vibration control story $K_{2,M05A}$ was given by using the optimal tuning design formula based on the fixed-point theory (Den Hartog 1956) for the 2DOF system of Case M05A. Thus, $K_{2,M05A}$ was calculated to be 62.2 MN/m. From the obtained $K_{2,M05A}$, the necessary number of STP units was calculated using the horizontal stiffness data of the STP specimen described above ($K_{eq,STP}$ = 0.56 MN/m). As a result, a total of 111 STP units were placed in the vibration control story of the model. The lateral stiffness of the vibration control story $K_{2,M05A}$ was expressed as:

$$K_{2,M05A} = 62.2 \text{ MN/m} = K_{eq,STP} \times 111 \text{ units.} \quad (1)$$

Then, the total lateral viscous damping coefficient of the vibration control story $C_{2,M05A}$ was set based on the values of the equivalent viscous damping factor ($h_{eq,STP}$ = 0.17) and the equivalent stiffness ($K_{eq,STP}$ = 0.56 MN/m) in the horizontal direction, as obtained from the experiment results for the STP specimen. The lateral viscous damping coefficient of the vibration control story $C_{2,M05A}$ was calculated as:

$$C_{2,M05A} = 2 \times h_{eq,STP} (\text{M2} \times K_{eq,STP} \times 111 \text{ units})^{0.5} = 1.695 \text{ MNs/m.} \quad (2)$$

Moreover, to consider the cases when the structural parameters of STP units in the vibration control system changed or differed from those of Case M05A due to the dependencies shown in the experiment and factors such as wear, fatigue, or aging, an additional four analytical cases (i.e., Cases M05B–M05E) were modeled with increased or decreased lateral equivalent stiffness

and viscous damping factor compared to those of the benchmark (Case M05A).

For Case M05B, decreased lateral stiffness $K_{2,\mathrm{M05B}}$ and viscous damping coefficient $C_{2,\mathrm{M05B}}$ were set by multiplying both $K_{\mathrm{eq,STP}}$ and $h_{\mathrm{eq,STP}}$ by 0.5. For Case M05C, lateral stiffness $K_{2,\mathrm{M05C}}$ was increased by multiplying $K_{\mathrm{eq,STP}}$ by 2.0, and lateral viscous damping coefficient $C_{2,\mathrm{M05C}}$ was calculated by multiplying $h_{\mathrm{eq,STP}}$ by 0.5. For Case M05D, lateral stiffness $K_{2,\mathrm{M05D}}$ was decreased by multiplying $K_{\mathrm{eq,STP}}$ by 0.5, and lateral viscous damping coefficient $C_{2,\mathrm{M05D}}$ was obtained by multiplying $h_{\mathrm{eq,STP}}$ by 2.0. For Case M05E, increased lateral stiffness $K_{2,\mathrm{M05E}}$ and viscous damping coefficient $C_{2,\mathrm{M05E}}$ were set by multiplying both $K_{\mathrm{eq,STP}}$ and $h_{\mathrm{eq,STP}}$ by 2.0. The other parameters, M1, K1, and M2, of Cases M05B–M05E were set to be the same as those of Case M05A. The properties of each analytical model for Cases M05A–M05E are given in Table 4.1.

Similarly, parameters for Cases M10A–M10E were calculated using the same approach as used for Cases M05A–M05E described above, except with the mass ratio given as 0.1. For Case M10A, the total lateral stiffness $K_{2,\mathrm{M10A}}$ and viscous damping coefficient $C_{2,\mathrm{M10A}}$ of the vibration control story were calculated as follows, and the necessary number of STP units was calculated to be 202 units:

$$K_{2,\mathrm{M10A}} = 113.3 \text{ MN/m} = K_{\mathrm{eq,STP}} \times 202 \text{ units}, \quad (3)$$

$$C_{2,\mathrm{M10A}} = 2 \times h_{\mathrm{eq,STP}} (\mathrm{M2} \times K_{\mathrm{eq,STP}} \times 202 \text{ units})^{0.5} = 3.237 \text{ MNs/m}. \quad (4)$$

The generated parameters for Cases M10A–M10E are also shown in Table 4.1.

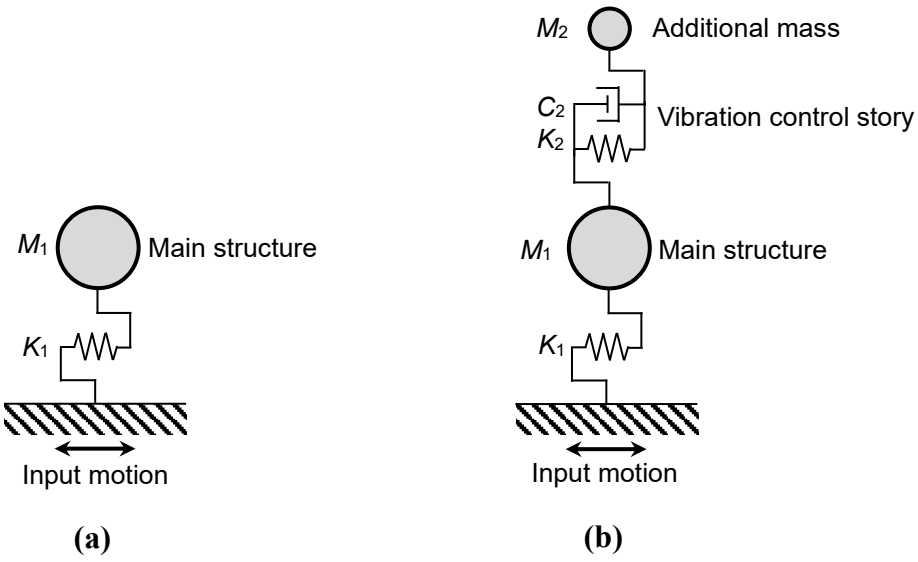

Figure 4.1 Numerical structure models: (a) non-controlled model (SDOF system); and (b) controlled model (2DOF system)

Table 4.1 Properties of the analytical models

Case	M_1 (t)	K_1 (MN/m)	Mass ratio (%)	M_2 (t)	K_2 (MN/m)	C_2 (MNs/m)
N	8,000	1,371	-	-	-	-
M05A	8,000	1,371	5	400	62.2	1.695
M05B	8,000	1,371	5	400	31.1	0.599
M05C	8,000	1,371	5	400	124.3	1.199
M05D	8,000	1,371	5	400	31.1	2.398
M05E	8,000	1,371	5	400	124.3	4.795
M10A	8,000	1,371	10	800	113.3	3.237
M10B	8,000	1,371	10	800	56.6	1.144
M10C	8,000	1,371	10	800	226.6	2.289
M10D	8,000	1,371	10	800	56.6	4.578
M10E	8,000	1,371	10	800	226.6	9.155

2.3 Ground motion input

A total of 10 observed earthquakes, whose peak ground velocities (PGVs) were normalized to 0.5 m/s, were used for ground motion input. Peak ground acceleration (PGA) of the input motions are listed in Table 4.2. Two (Kobe 1995 NS and EW) of the 10 seismic patterns were based on public data from the Japan Meteorological Agency. The other eight waves (El Centro 1940, Taft 1952, Hachinohe 1968, and Tohoku 1978 in both the NS and EW directions) were based on wave data provided by the Building Performance Standardization Association of Japan. Figure 4.2 shows velocity response spectra for the input motions with a damping factor of 0.05.

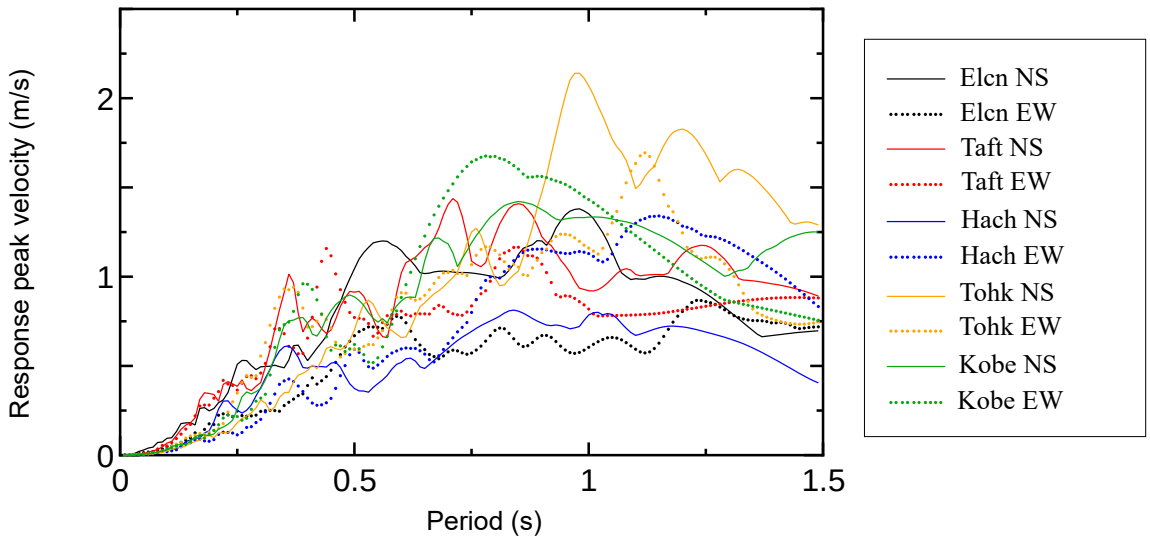

Figure 4.2 Velocity response spectra of input motions (damping factor 0.05) (Elcn = El Centro, Hach = Hachinohe, Tohk = Tohoku)

Table 4.2 Input earthquake motions

Wave name *	Original observed record	PGV (m/s)	PGA (cm/s^2)
Elcn NS	1940 El Centro NS	0.5	510.0
Elcn EW	1940 El Centro EW	0.5	284.7
Taft NS	1952 Taft NS	0.5	486.3
Taft EW	1952 Taft EW	0.5	496.9
Hach NS	1968 Hachinohe NS	0.5	333.8
Hach EW	1968 Hachinohe EW	0.5	238.4
Tohk NS	1978 Tohoku NS	0.5	356.5
Tohk EW	1978 Tohoku EW	0.5	368.5
Kobe NS	1995 Kobe NS	0.5	446.0
Kobe EW	1995 Kobe EW	0.5	413.2

* Elcn = El Centro, Hach = Hachinohe, Tohk = Tohoku

2.4 Analytical conditions

For each analytical case, stiffness proportional viscous damping (damping factor = 2%) was adopted for structural damping of the whole system. The Newmark-β method (β = 1/4) was used for numerical integration. A time increment of 0.005 s was used.

3. Analytical results and discussion

3.1 Results of eigenvalue analysis

Table 4.3 lists the natural period and frequency for the first and second mode for each case obtained by eigenvalue analysis. The table also shows the damping factor obtained by complex eigenvalue analysis. The natural period and damping factor for the main structure alone (Case N) were 0.48 s and 2%, respectively. The damping factors of the first mode for Cases M05A, M05B, and M05D showed larger values, 9.8% or more, whereas smaller damping factors were obtained for Cases M05C and M05E in the first mode. Similarly, the damping factors in the first mode for Cases M10A, M10B, and M10D exceeded 9.4%, whereas those for Cases M10C and M10E resulted in smaller values.

Table 4.3 Results of eigenvalue analysis

Case	Mode	Natural period (s)	Natural frequency (Hz)	Damping factor * (%)
N	1	0.48	2.08	2.0
M05A	1	0.55	1.82	10.5
	2	0.44	2.27	11.4
M05B	1	0.73	1.38	9.8
	2	0.47	2.12	3.9
M05C	1	0.50	1.99	2.4
	2	0.34	2.94	11.2
M05D	1	0.73	1.38	34.4
	2	0.47	2.12	5.4
M05E	1	0.50	1.99	3.2
	2	0.34	2.94	36.5
M10A	1	0.59	1.70	10.8
	2	0.43	2.33	11.7
M10B	1	0.77	1.30	9.4
	2	0.46	2.15	4.7
M10C	1	0.53	1.90	2.8
	2	0.34	2.94	11.1
M10D	1	0.77	1.30	33.2
	2	0.46	2.15	7.5
M10E	1	0.53	1.90	4.3
	2	0.34	2.94	36.3

* As obtained by complex eigenvalue analysis

3.2 Results of earthquake response analysis

Figure 4.3 plots the peak acceleration response reduction ratios of the main structure for Cases M05A and M10A to Case N against each input motion obtained from the earthquake response analysis. Similarly, the peak displacement response reduction ratios for Cases M05A and M10A to Case N are shown in Figure 4.4. The results for Case M05A with 5% mass ratio demonstrated that installing the proposed control system reduced the peak response effectively for all input earthquakes compared to non-controlled Case N. Moreover, the results for Case M10A with 10% mass ratio exhibited a better reduction than those for Case M05A. The mean of the acceleration reduction ratios for the 10 input motions in Cases M05A and M10A were 0.704 and 0.612, respectively, and those of the displacement were 0.740 and 0.667, respectively. Also, the coefficient of variation of the acceleration reduction ratios for the 10 earthquakes in Cases M05A and M10A were 0.169 and 0.139, respectively, and those of the displacement were 0.163 and 0.146, respectively. From this, the results with the mass ratio of 10% (Case M10A) gave smaller coefficient of variation values, as well as mean values, compared to those with the mass ratio of 5% (Case M05A).

Tables 4.4 and 4.5 respectively list the average peak response acceleration and displacement of the structure, which were obtained as averages of the responses to the 10 input motions, for each analytical model. Also, response reduction ratios for each controlled model (Cases M05A–M05E and M10A–M10E) to the non-controlled model (Case N) for the average peak response acceleration and displacement of the main structure are given in Tables 4.4 and 4.5, respectively. Moreover, the means of these results averaged for each mass ratio are shown in Tables 4.4 and 4.5. These results showed that both maximum response acceleration and displacement of the main structure in the controlled models (Cases M05A–M05E and M10A–M10E) were obviously reduced as compared to those for the non-controlled model (Case N). Among the controlled models with 5% mass ratio, Case M05A yielded the most promising results, and the other controlled models (Cases M05B–05E) gave fairly good response reduction effects compared to the non-controlled model (Case N). This means that there would be a relatively small decrease of the control effect even if the lateral equivalent stiffness and

damping factor of the STPs vary within the fluctuation range adopted in this analysis. Similarly, Case M10A produced the most promising reduction among the controlled models with 10% mass ratio. Moreover, the results for the mass ratio of 10% (Cases M10A–M10E) generally gave better response control effects in comparison with those for the mass ratio of 5% (Cases M05A–M05E).

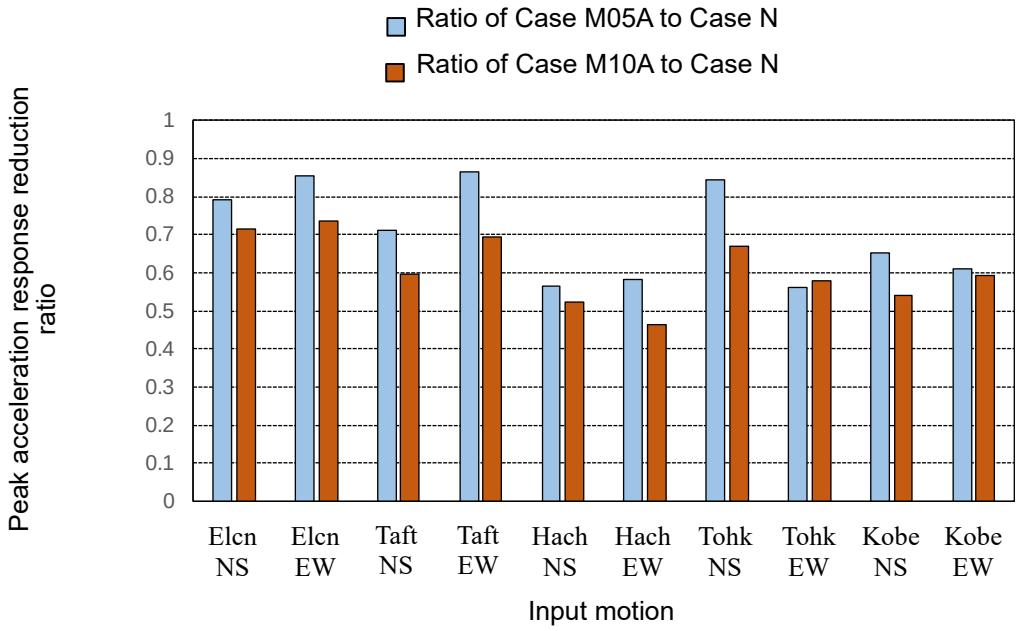

Figure 4.3 Response reduction ratios of Case M05A and Case M10A with respect to Case N for peak acceleration of main structure

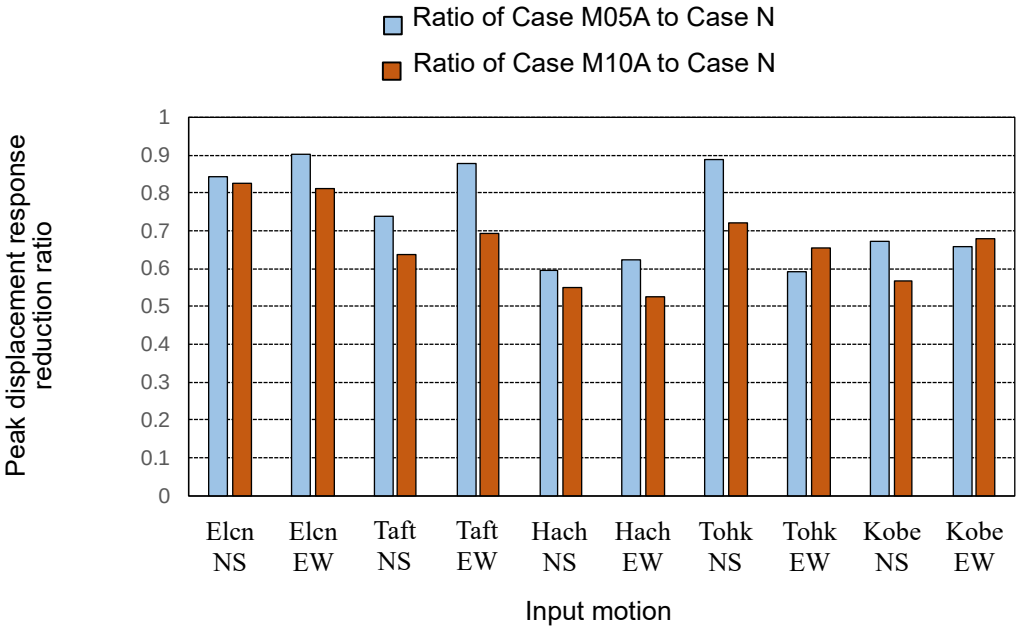

Figure 4.4 Response reduction ratios of Case M05A and Case M10A with respect to Case N for peak displacement of main structure

Table 4.4 Peak acceleration obtained by earthquake response analysis

Case	Peak acceleration of main structure *1 (m/s^2)	Reduction ratio *2	Peak acceleration of vibration control system *1 (m/s^2)
N	12.24	-	-
M05A	8.61	0.70	19.27
M05B	9.89	0.81	14.87
M05C	10.33	0.84	20.99
M05D	9.28	0.76	10.48
M05E	10.32	0.84	15.86
Average for M05A–M05E	**9.69**	**0.79**	**16.29**
M10A	7.48	0.61	15.15
M10B	9.11	0.74	13.23
M10C	9.26	0.76	19.27
M10D	8.29	0.68	9.16
M10E	9.19	0.75	14.05
Average for M10A–M10E	**8.67**	**0.71**	**14.17**

*1 Peak response value (mean for 10 input motions)
*2 Ratio of peak acceleration of main structure for each controlled model (mean for 10 input motions) to that for non-controlled model

Table 4.5 Peak displacement obtained by earthquake response analysis

Case	Peak story drift of main structure *1 (mm)	Reduction ratio *2	Peak story drift of vibration control story *1 (mm)
N	71.35	-	-
M05A	52.68	0.74	116.06
M05B	56.56	0.79	185.53
M05C	65.71	0.92	66.61
M05D	54.73	0.77	101.52
M05E	64.44	0.90	45.11
Average for M05A–M05E	**58.82**	**0.82**	**102.97**
M10A	47.56	0.67	100.27
M10B	51.72	0.72	181.38
M10C	63.61	0.89	67.03
M10D	50.09	0.70	97.94
M10E	61.06	0.86	43.79
Average for M10A–M10E	**54.81**	**0.77**	**98.08**

*1 Peak response value (mean for 10 input motions)
*2 Ratio of peak story drift of main structure for each controlled model (mean for 10 input motions) to that for non-controlled model

4. Conclusions

An earthquake response analysis using SDOF and 2DOF models with mass ratios of 5% or 10% was carried out to evaluate the response reduction effects when applying the proposed seismic mass damper system to a structure. The results demonstrated the effectiveness of the proposed system in reduction of peak response acceleration and displacement of the main structure against various input motions compared to those without the vibration control system.

In the response analysis, three-dimensional effects including vertical, rotational, or torsional behaviour of the STP units were not considered. These effects should be investigated in future work. Studies on used tires whose mileage is much higher (e.g., 50,000 km) than those used in this study are also included in future challenges.

References

[1] Building Performance Standardization Association. (in Japanese) (Access date: July 30, 2019)
https://www.seinokyo.jp/jsh/top/

[2] Den Hartog JP (1956) Mechanical vibrations (4th ed.), McGraw-Hill, New York.

[3] Japan Meteorological Agency. (in Japanese) (Access date: July 30, 2019)
https://www.data.jma.go.jp/svd/eqev/data/kyoshin/jishin/hyogo_nanbu/index.html

[4] Park J, Shirai K, Kikuchi M (2017) A proposal of a seismic mass damper system using waste tires appropriate for RC building structures part 3 analyzing experimental data and earthquake response analysis, Summaries of Technical Papers of Annual Meeting, Architectural Institute of Japan, Structure II, 745-746. (in Japanese)

[5] Shirai K, Kikuchi M (2015) A proposal of a seismic mass damper system using waste tires appropriate for RC building structures, Summaries of Technical Papers of Annual Meeting, Architectural Institute of Japan, Structure IV, 609-610. (in Japanese)

[6] Shirai K, Park J, Kikuchi M (2017) A proposal of a seismic mass damper system using waste tires appropriate for RC building structures part 2 methods and results of loading tests on a STP specimen, Summaries of Technical Papers of Annual Meeting, Architectural Institute of Japan, Structure II, 743-744. (in Japanese)

[7] Shirai K, Park J (2020) Use of scrap tire pads in vibration control system for seismic response reduction of buildings, Bulletin of Earthquake Engineering, 18(5), 2497–2521.
https://doi.org/10.1007/s10518-020-00787-2

Chapter V

Numerical assessment of control effects for nonlinear multi-story building models

The contents of this Chapter V have been published in the following paper.

Park J, Shirai K, Kikuchi M, "A seismic mass damper system using scrap tire pads: Loading tests on mechanical properties and numerical assessment of the response control effects", Soil Dynamics and Earthquake Engineering, vol. 157, 107257, 2022.

Numerical assessment of control effects for nonlinear multi-story building models

1. Introduction

The present study aimed to evaluate the response control effects achieved by the seismic mass damper (SMD) system using scrap tire pads (STPs). Numerical response was obtained for six- and 10-story building models incorporating the SMD system using STPs subjected to various earthquakes.

2. Analytical methods

2.1 Description of six-story reinforced-concrete building models and ten-story steel-reinforced-concrete building models

A numerical seismic response simulation was conducted in order to evaluate the control effects of the SMD system using STPs for multi-story building models. Figure 5.1 shows the numerical vibrating models used in the analysis. The analytical models were prepared with reference to two building models considering soil-structure interaction. One is a six-story reinforced-concrete building based on data from Architectural Institute of Japan (2006) and Shirai et al. (2021) and the other is a 10-story steel-reinforced-concrete building based on data provided by Architectural Institute of Japan (2006). The six- and 10-story buildings are hereinafter referred to as the 6S and 10S series, respectively. As shown in Figure 5.2, a degrading trilinear restoring force characteristic (Takeda. 1974) with an unloading parameter $\gamma = 0.5$ was set to the shear spring in each story of the superstructure for each of the 6S and 10S series.

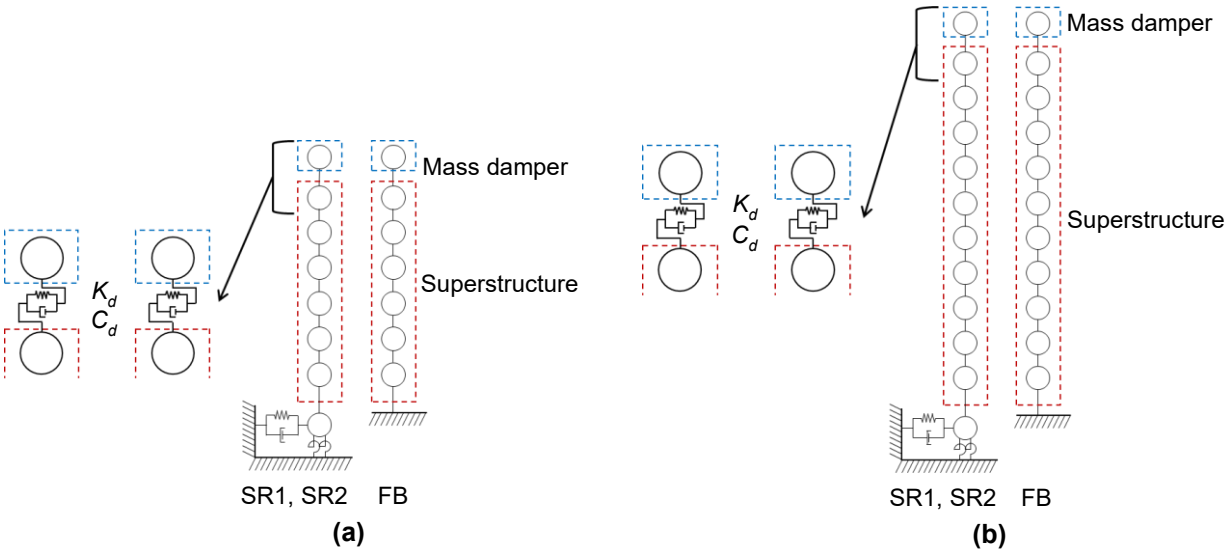

Figure 5.1 Numerical structure models: (a) 6S series (six-story building); and (b) 10S series (10-story building)

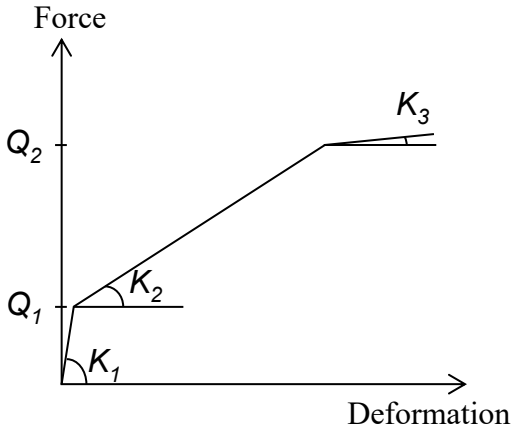

Figure 5.2 Restoring force characteristics of the nonlinear shear spring for each story of the superstructure

2.1.1 Modeling of main structure

Tables 5.1 and 5.2 list the specifications of the nonlinear shear spring for each story of the superstructure for the 6S and 10S series, respectively. Here, K_1, K_2, and K_3 denote the initial stiffness, the stiffness after cracking, and the stiffness after yielding, respectively. Moreover, Q_1 and Q_2 denote the shear force at the cracking and yielding points, respectively. For each series, three types of the foundation condition were adopted. One is a model with a fixed-base condition, hereinafter referred as the FB type. The others are models considering sway-rocking motion, hereinafter referred as the SR1 and SR2 types, by placing springs and damping elements for sway and rocking motion under the superstructure. The superstructure for FB, SR1, and SR2 types were identical in each series (6S and 10S). Tables 5.3 and 5.4 give the specifications of the springs and viscous damping elements for sway and rocking motion of SR1 and SR2 types for each series, respectively.

Table 5.1 Properties of the superstructure for the 6S series (six-story building)

Story	Height [m]	Weight [kN]	K_1 [kN/m]	K_2 [kN/m]	K_3 [kN/m]	Q_1 [kN]	Q_2 [kN]
6	2.85	4,681	2,220,000	313,000	2,500	1,567	3,536
5	2.85	4,902	2,420,000	350,000	12,700	2,403	5,598
4	2.85	4,902	2,470,000	407,000	31,900	2,819	6,949
3	2.85	5,096	2,580,000	477,000	44,400	3,319	8,239
2	2.85	5,096	2,360,000	483,000	50,600	4,530	9,514
1	3.45	5,100	3,050,000	510,000	35,000	5,062	11,383
Foundation	-	7,792	-	-	-	-	-

Table 5.2 Properties of the superstructure for the 10S series (10-story building)

Story	Height [m]	Weight [kN]	K_1 [kN/m]	K_2 [kN/m]	K_3 [kN/m]	Q_1 [kN]	Q_2 [kN]
10	3.8	18,780	5,960,000	2,830,000	209,000	14,100	29,700
9	3.8	17,490	8,330,000	3,210,000	132,000	16,600	48,500
8	3.8	17,470	10,200,000	4,440,000	314,000	17,700	57,600
7	3.8	17,570	11,800,000	5,420,000	445,000	19,000	64,400
6	3.8	17,600	14,000,000	6,580,000	513,000	24,400	71,100
5	3.8	17,840	16,000,000	7,760,000	599,000	24,300	75,800
4	3.8	17,820	18,100,000	8,730,000	674,000	26,400	79,900
3	3.8	17,940	22,200,000	15,700,000	706,000	33,200	84,500
2	4.2	18,910	28,800,000	24,800,000	623,000	28,000	93,900
1	4.5	24,670	38,500,000	36,900,000	1,460,000	40,400	99,600
Foundation	-	59,430	-	-	-	-	-

Table 5.3 Specifications of the sway and rocking motions for the 6S series (six-story building)

Element	Unit	SR1	SR2
Sway stiffness	kN/m	610,000	240,000
Sway damping coefficient	kNs/m	26,900	46,300
Rocking stiffness	kNm/rad	1.88×10^9	1.83×10^9
Rocking damping coefficient	kNms/rad	11,800,000	16,300,000

Table 5.4 Specifications of the sway and rocking motions for the 10S series (10-story building)

Element	Unit	SR1	SR2
Sway stiffness	kN/m	9,550,000	7,590,000
Sway damping coefficient	kNs/m	294,000	625,000
Rocking stiffness	kNm/rad	1.72×10^{10}	1.14×10^{10}
Rocking damping coefficient	kNms/rad	217,000,000	230,000,000

2.1.2 Modeling of vibration control system

Four different control cases, hereinafter referred to as cases N, C1, C2, and C3, were investigated for each type and each series. Case N represents a non-controlled case without an SMD, whereas cases C1, C2, and C3 represent controlled cases in which an SMD using STPs is installed on the roof of case N. A total of 24 models (= 2 series × 3 types × 4 cases) was prepared and used in the analysis. Hereinafter, the numerical models are referred to by a combination of series-type-case, such as models 6S-FB-N and 10S-SR1-C2. The additional mass of the SMD was given such that the mass ratio, μtotal, was 5.0% for each controlled case (C1, C2, and C3), where μ_{total} is the ratio of the SMD additional mass to the total mass of the superstructure. As a result, the mass ratio, μ_{eff}, which is a ratio of the SMD additional mass to the first modal effective mass of the superstructure, distributed within 5.0% to 7.0% among all controlled models. Based on the loading test results (surface pressure 1.0 MPa, loading displacement 20 mm, loading frequency 2.0 Hz) in Chapter III, an equivalent stiffness of $K_{\text{eq,STP}}$ = 560 kN/m and an equivalent damping factor of $h_{\text{eq,STP}}$ = 0.17 were assumed for the lateral property of a single STP unit in the numerical models. For models 6S-FB-C1, C2, and C3, the property of the mass damper story was given as follows. Regarding model 6S-FB-C1, the total lateral stiffness, K_{d}, of the mass damper story was set using the optimal tuning formula for TMDs based on the fixed-point theory (Den Hartog. 1956) as

$$\nu_{\text{opt}} = 1/(1 + \mu_{\text{eff}}) \tag{1}$$

where ν_{opt} is the optimal frequency ratio for the natural frequency of the mass damper alone to the first modal natural frequency of the building without an SMD.

Then, the required number of STP units, N_{d}, was obtained from the assumed

$K_{eq,STP}$ (= 560 kN/m) [Eqs. (2) and (3)]. In addition, the total lateral damping coefficient, C_d, of the mass damper story was calculated using $h_{eq,STP}$ (= 0.17) and $K_{eq,STP}$ [Eq. (4)]. For model 6S-FB-C1, the total lateral stiffness (K_d), the required number of STPs units (N_d), and the total lateral damping coefficient (C_d) of the mass damper story were calculated as

$$K_d = 41{,}287 \text{ kN/m} \quad (2)$$

$$N_d = K_d / K_{eq,STP} = 74 \text{ units} \quad (3)$$

$$C_d = 2\, h_{eq,STP}\, (M_d\, K_d)^{0.5} = 851.5 \text{ kNs/m} \quad (4)$$

where M_d is the mass of the SMD additional mass (= 151.9 t).

Moreover, the other control cases (i.e., cases C2 and C3) with reduced K_d and C_d were prepared in order to consider the effect of progressed nonlinearity of the superstructure due to the increase in response deformation. The reduced K_d and C_d for case C2 were obtained by multiplying the values for case C1 by 0.5. In addition, the reduced K_d and C_d for case C3 were obtained by multiplying the values for case C1 by 0.25. A similar calculation procedure of the mass damper story properties for models 6S-FB-C1, C2, and C3 described the above was adopted for the other controlled models. The specifications of the mass damper story for the 6S and 10S series are given in Tables 5.5 and 5.6, respectively. In the analysis, for the mass damper story, each STP unit was supposed to be fixed using an adhesive to the lower slab (i.e., the roof of the building superstructure) and the upper slab (i.e., the additional mass). A linear model was used for the horizontal shear spring representing the STP units for simplicity. Slippage and rollover deformation between the STP units and the upper and lower slabs were not considered.

Table 5.5 Properties of the mass damper story for the 6S series (six-story building)

Model	M_d [kN]	K_d [kN/m]	C_d [kNs/m]
6S-FB-N	without mass damper		
6S-FB-C1	1,489.9	41,286.7	851.5
6S-FB-C2	1,489.9	20,643.4	425.8
6S-FB-C3	1,489.9	10,321.7	212.9
6S-SR1-N	without mass damper		
6S-SR1-C1	1,489.9	15,565.7	522.8
6S-SR1-C2	1,489.9	7,782.9	261.4
6S-SR1-C3	1,489.9	3,891.4	130.7
6S-SR2-N	without mass damper		
6S-SR2-C1	1,489.9	7,505.7	363.1
6S-SR2-C2	1,489.9	3,752.9	181.5
6S-SR2-C3	1,489.9	1,876.4	90.8

Table 5.6 Properties of the mass damper story for the 10S series (10-story building)

Model	M_d [kN]	K_d [kN/m]	C_d [kNs/m]
10S-FB-N	without mass damper		
10S-FB-C1	9,304.5	192,608.7	4,596.2
10S-FB-C2	9,304.5	96,304.4	2,298.1
10S-FB-C3	9,304.5	48,152.2	1,149.1
10S-SR1-N	without mass damper		
10S-SR1-C1	9,304.5	137,404.2	3,882.1
10S-SR1-C2	9,304.5	68,702.1	1,941.0
10S-SR1-C3	9,304.5	34,351.0	970.5
10S-SR2-N	without mass damper		
10S-SR2-C1	9,304.5	126,260.1	3,721.3
10S-SR2-C2	9,304.5	63,130.1	1,860.7
10S-SR2-C3	9,304.5	31,565.0	930.3

2.2 Ground motion input

Table 5.7 lists the input motions used in the analysis. Ten observed records (Japan Meteorological Agency. 2019; Building Performance Standardization Association) and five simulated waves (Shirai and Inoue. 2014) were adopted as the input motions. For the observed records, each waveform was normalized such that the peak ground velocity (PGV) was 0.5 m/s. Each simulated wave was fitted to the same target response spectrum (damping factor of 0.05) and had different phase characteristics using random numbers. Figure 5.3 depicts the response velocity spectra of the observed records and simulated waves.

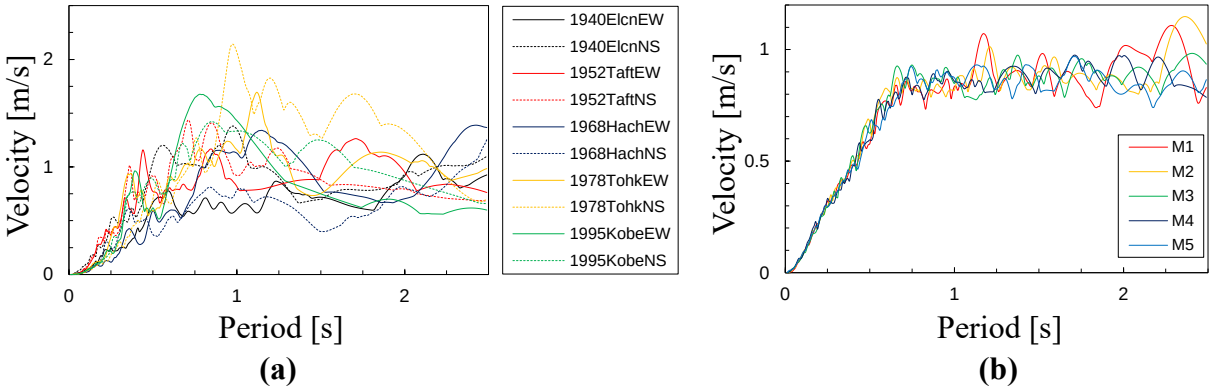

Figure 5.3 Velocity response spectra of the input motions (damping factor: 0.05): (a) 10 observed records (Elcn = El Centro, Hach = Hachinohe, Tohk = Tohoku) (peak ground velocity 0.5 m/s); and (b) five simulated waves

Table 5.7 Input motions used in the numerical simulation

Wave group	Wave name	Original record	PGA [cm/s^2]
Observed records (PGV = 50 cm/s)	Elcn NS	1940 El Centro NS	510.0
	Elcn EW	1940 El Centro EW	284.7
	Taft NS	1952 Taft NS	486.3
	Taft EW	1952 Taft EW	496.9
	Hach NS	1968 Hachinohe NS	333.8
	Hach EW	1968 Hachinohe EW	238.4
	Tohk NS	1978 Tohoku NS	356.5
	Tohk EW	1978 Tohoku EW	368.5
	Kobe NS	1995 Kobe NS	446.0
	Kobe EW	1995 Kobe EW	413.2
Simulated waves	M1	-	419.0
	M2	-	380.0
	M3	-	339.0
	M4	-	339.0
	M5	-	314.0

PGA: peak ground acceleration
PGV: peak ground velocity

2.3 Analytical conditions

Structural damping was adopted for each of the 6S and 10S series as follows. First, a dashpot for the horizontal shear direction was set at each story of the superstructure of model FB-N, so that a damping factor of 0.005 for the first mode (an initial stiffness proportional-type damping) was obtained. Then, the identical dashpot was placed at each story of the other models (i.e., models FB-C1–C3, SR1-N and C1–C3, and SR2-N and C1–C3). The Newmark-β method (β = 1/4) with a time interval of 0.001 s was used.

3. Analytical results and discussion

3.1 Results of eigenvalue analysis

From an eigenvalue analysis, Tables 5.8 and 5.9 show the first modal natural period and frequency of each model for the 6S and 10S series, respectively. Moreover, the first modal damping factors obtained from a complex eigenvalue analysis for models 6S-FB-N, C1, C2, and C3 were 0.5%, 7.9%, 10.3%, and 8.1%, respectively. From these results, installation of the SMD (i.e., the controlled cases) significantly increased the first modal damping factor as compared to the case without the SMD (i.e., the non-controlled case) for the FB type.

Table 5.8 Natural period and frequency for the first mode of the 6S series (six-story building)

Model	Natural period [s]	Natural frequency [Hz]
6S-FB-N	0.36	2.78
6S-FB-C1	0.43	2.31
6S-FB-C2	0.56	1.79
6S-FB-C3	0.77	1.29
6S-SR1-N	0.59	1.69
6S-SR1-C1	0.68	1.46
6S-SR1-C2	0.90	1.11
6S-SR1-C3	1.25	0.80
6S-SR2-N	0.85	1.17
6S-SR2-C1	0.97	1.03
6S-SR2-C2	1.29	0.78
6S-SR2-C3	1.80	0.56

Table 5.9 Natural period and frequency for the first mode of the 10S series (10-story building)

Model	Natural period [s]	Natural frequency [Hz]
10S-FB-N	0.41	2.43
10S-FB-C1	0.51	1.94
10S-FB-C2	0.66	1.52
10S-FB-C3	0.90	1.11
10S-SR1-N	0.49	2.04
10S-SR1-C1	0.60	1.67
10S-SR1-C2	0.77	1.30
10S-SR1-C3	1.06	0.94
10S-SR2-N	0.51	1.95
10S-SR2-C1	0.62	1.61
10S-SR2-C2	0.80	1.25
10S-SR2-C3	1.11	0.90

3.2 Results of earthquake response analysis

Tables 5.10 and 5.11 show the peak acceleration and story drift response, respectively, of the superstructure for the 6S series. Here, the peak response is the mean for each input motion group (i.e., averaged for the 10 observed records and for the five simulated waves). In addition, the peak response of the superstructure is the maximum value in all stories of the superstructure excluding the mass damper. As shown in Table 5.11, for each input motion group of the 6S series, as compared with the non-controlled cases (N), a clear reduction was demonstrated in the peak story drift responses of the superstructure for the control cases (C1, C2, and C3). Similar to Tables 5.10 and 5.11, the peak acceleration and story drift response of the superstructure for the 10S series are shown in Tables 5.12 and 5.13, respectively. From Table 5.13, for the 10S series, the peak story drift responses of the superstructure for the controlled cases were reduced as compared with those for the non-controlled cases, except for models 10S-SR1-C1 and 10S-SR2-C1 for the observed records input. By adopting the reduced K_d and C_d in controlled cases C2 and C3, this lack of reduction observed in models 10S-SR1-C1 and 10S-SR2-C1 was improved. Moreover, the peak response acceleration and story drift of the mass damper story are also shown in Tables 5.10–5.13. From Tables 5.11 and 5.13, a tendency was observed whereby the story drift at the SMD increased as K_d and C_d were reduced.

Figure 5.4 and Figure 5.5 plot the ratio of the peak acceleration and story drift response, respectively, for each controlled case (C1, C2, and C3) to those of the non-controlled case (N) for the 6S series. Here, the peak response is the maximum value in all stories of the superstructure excluding the mass damper, and the ratios are averaged in each input motion group (10 observed records and five simulated waves). Similarly, Figure 5.6 and Figure 5.7 show the ratio of the peak acceleration and story drift response, respectively, for the 10S series. From Figures 5.5 and 5.7, for the 6S and 10S series, the ratios

for the peak story drift were less than unity, except for the 6S-FB-C2 model for the simulated waves input and the 10S-SR1-C1 and 10S-SR2-C1 models for the observed records input. The averaged values of the ratios of the peak story drift for each model of the 6S and 10S series (i.e., mean for the 18 values in each of Figure 5.5 and 5.7) were 0.874 and 0.826, respectively. This showed the effectiveness of the response reduction in the story drift of the superstructure by the SMD system using STPs.

In addition, as a method to consider the fluctuation of the mechanical properties of the STP units in seismic response assessment, a numerical simulation was conducted by setting parameters as a combination of the upper and/or lower boundaries of the variation of the equivalent stiffness and damping factor for the STP units (Shirai and Park. 2020). Such an approach may be useful to assess the response control effect of the SMD system using the STP units in consideration of the deterioration of the STPs.

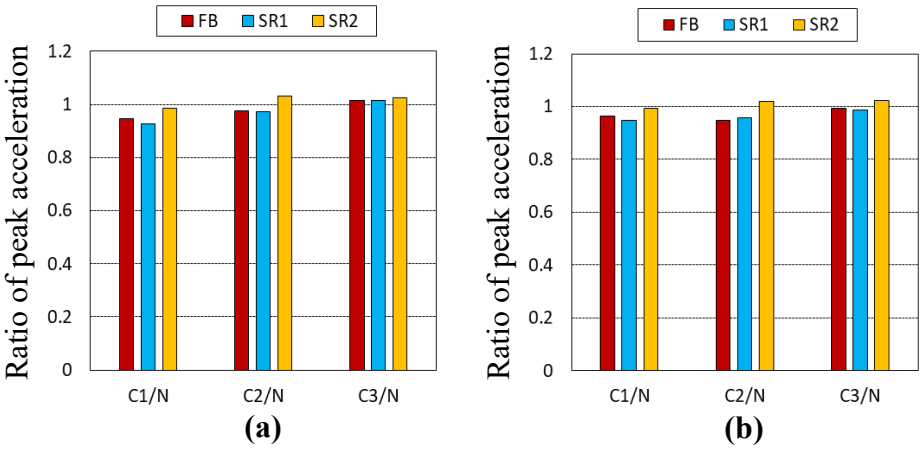

Figure 5.4 Ratio of the peak response acceleration of each controlled case to that of the non-controlled case for the 6S series (maximum value for all stories of the superstructure excluding the mass damper): (a) mean for the 10 observed records; and (b) mean for the five simulated waves

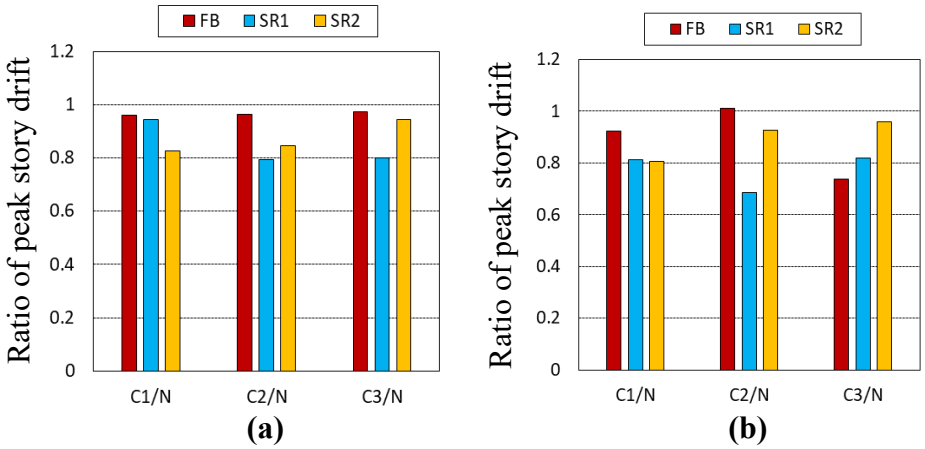

Figure 5.5 Ratio of the peak response story drift of each controlled case to that of the non-controlled case for the 6S series (maximum value for all stories of the superstructure excluding the mass damper): (a) mean for the 10 observed records; and (b) mean for the five simulated waves

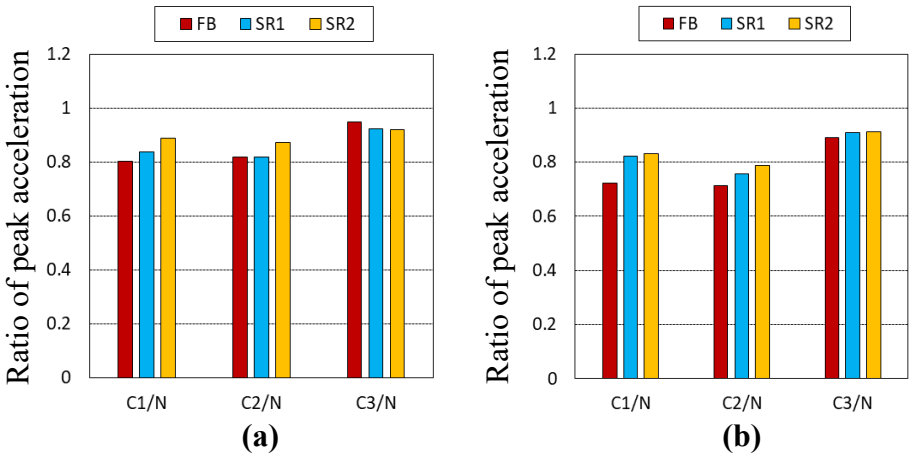

Figure 5.6 Ratio of the peak response acceleration of each controlled case to that of the non-controlled case for the 10S series (maximum value for all stories of the superstructure excluding the mass damper): (a) mean for the 10 observed records; and (b) mean for the five simulated waves

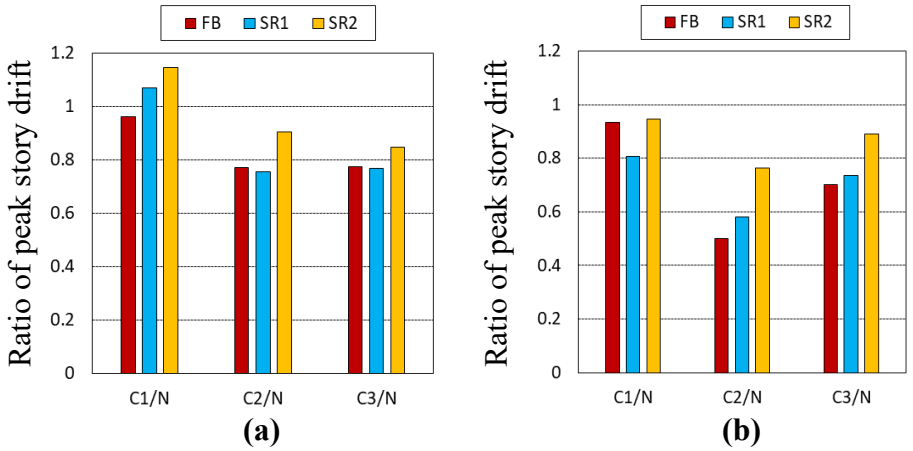

Figure 5.7 Ratio of the peak response story drift of each controlled case to that of the non-controlled case for the 10S series (maximum value for all stories of the superstructure excluding the mass damper): (a) mean for the 10 observed records; and (b) mean for the five simulated waves

Table 5.10 Peak acceleration obtained from the earthquake response analysis for the 6S series (six-story building)

Model	Observed records input *1		Simulated waves input *2	
	Peak acceleration of superstructure *3 [m/s^2]	Peak acceleration of mass damper [m/s^2]	Peak acceleration of superstructure *3 [m/s^2]	Peak acceleration of mass damper [m/s^2]
6S-FB-N	6.27	-	6.45	-
6S-FB-C1	5.92	8.69	6.23	8.63
6S-FB-C2	6.09	10.53	6.12	11.37
6S-FB-C3	6.35	13.49	6.40	13.65
6S-SR1-N	6.32	-	6.03	-
6S-SR1-C1	5.83	9.25	5.67	9.44
6S-SR1-C2	6.15	12.17	5.75	10.25
6S-SR1-C3	6.44	9.23	5.96	6.74
6S-SR2-N	6.33	-	6.50	-
6S-SR2-C1	6.23	10.18	6.45	8.23
6S-SR2-C2	6.53	6.88	6.62	5.25
6S-SR2-C3	6.49	3.61	6.64	3.23

*1 Mean for the 10 observed records
*2 Mean for the five simulated waves
*3 Maximum value for all stories of the superstructure excluding the mass damper

Table 5.11 Peak story drift obtained from the earthquake response analysis for the 6S series (six-story building)

Model	Observed records input *1		Simulated waves input *2	
	Peak story drift of superstructure *3 [mm]	Peak story drift of mass damper [mm]	Peak story drift of superstructure *3 [mm]	Peak story drift of mass damper [mm]
6S-FB-N	37.1	-	26.2	-
6S-FB-C1	35.6	31.1	24.0	30.9
6S-FB-C2	35.1	76.0	26.0	82.0
6S-FB-C3	35.4	195.8	19.2	197.7
6S-SR1-N	39.0	-	23.5	-
6S-SR1-C1	36.5	87.2	18.9	88.5
6S-SR1-C2	31.9	231.3	16.3	193.7
6S-SR1-C3	31.3	353.8	19.3	258.0
6S-SR2-N	37.2	-	26.0	-
6S-SR2-C1	31.0	194.4	20.7	155.3
6S-SR2-C2	31.5	267.3	24.0	203.8
6S-SR2-C3	35.1	284.2	24.9	254.1

*1 Mean for the 10 observed records
*2 Mean for the five simulated waves
*3 Maximum value for all stories of the superstructure excluding the mass damper

Table 5.12 Peak acceleration obtained from the earthquake response analysis for the 10S series (10-story building)

Model	Observed records input *1		Simulated waves input *2	
	Peak acceleration of superstructure *3 [m/s^2]	Peak acceleration of mass damper [m/s^2]	Peak acceleration of superstructure *3 [m/s^2]	Peak acceleration of mass damper [m/s^2]
10S-FB-N	12.75	-	14.26	-
10S-FB-C1	10.22	16.21	10.23	16.94
10S-FB-C2	10.41	16.85	10.12	15.53
10S-FB-C3	12.18	12.82	12.63	9.55
10S-SR1-N	11.88	-	12.51	-
10S-SR1-C1	9.91	16.01	10.23	16.69
10S-SR1-C2	9.70	16.17	9.43	12.71
10S-SR1-C3	10.95	10.54	11.38	7.80
10S-SR2-N	10.26	-	10.51	-
10S-SR2-C1	9.01	14.37	8.61	14.09
10S-SR2-C2	8.85	13.77	8.27	10.02
10S-SR2-C3	9.40	8.74	9.57	6.30

*1 Mean for the 10 observed records
*2 Mean for the five simulated waves
*3 Maximum value for all stories of the superstructure excluding the mass damper

Table 5.13 Peak story drift obtained from the earthquake response analysis for the 10S series (10-story building)

Model	Observed records input *1		Simulated waves input *2	
	Peak story drift of superstructure *3 [mm]	Peak story drift of mass damper [mm]	Peak story drift of superstructure *3 [mm]	Peak story drift of mass damper [mm]
10S-FB-N	16.6	-	16.3	-
10S-FB-C1	15.2	77.0	14.8	80.4
10S-FB-C2	12.4	161.6	8.0	148.0
10S-FB-C3	12.4	247.6	11.2	184.0
10S-SR1-N	17.0	-	15.1	-
10S-SR1-C1	17.5	102.7	12.0	108.3
10S-SR1-C2	12.3	217.4	8.6	172.2
10S-SR1-C3	12.3	288.9	10.9	214.6
10S-SR2-N	12.4	-	9.6	-
10S-SR2-C1	14.2	99.1	9.0	97.3
10S-SR2-C2	10.6	201.9	7.3	148.2
10S-SR2-C3	9.9	262.6	8.5	189.7

*1 Mean for the 10 observed records
*2 Mean for the five simulated waves
*3 Maximum value for all stories of the superstructure excluding the mass damper

4. Conclusions

An earthquake response simulation was conducted using six- and 10-story numerical nonlinear building models including sway-rocking motion with and without an SMD system using STPs. The following conclusions were drawn.

1) From the results of the seismic response analysis, the effectiveness of the response reduction in the story drift of the superstructure by the SMD using STPs was exhibited for each of the six- and 10-story building models subjected to 10 observed records and five simulated waves. The averaged ratios of the peak response story drift of the controlled case to the non-controlled case for the six- and 10-story buildings were 0.874 and 0.826, respectively.
2) Adopting the reduced lateral stiffness (K_d) and damping coefficient (C_d) in the mass damper story may be useful for improving the performance of the response control effects considering the nonlinearity of the superstructure.

References

[1] Architectural Institute of Japan (2006) Seismic response analysis and design of buildings considering dynamic soil-structure interaction. Architectural Institute of Japan, Tokyo, Japan. (in Japanese)

[2] Building Performance Standardization Association. (in Japanese) (Access date: July 30, 2019)
https://www.seinokyo.jp/jsh/top/

[3] Den Hartog JP (1956) Mechanical vibrations (4th ed.). McGraw-Hill, New York.

[4] Japan Meteorological Agency. (in Japanese) (Access date: July 30, 2019)
https://www.data.jma.go.jp/svd/eqev/data/kyoshin/jishin/hyogo_nanbu/index.html

[5] Park J, Shirai K, Kikuchi M (2022) A seismic mass damper system using scrap tire pads: Loading tests on mechanical properties and numerical assessment of the response control effects, Soil Dynamics and Earthquake Engineering, vol. 157, 107257.
https://doi.org/10.1016/j.soildyn.2022.107257

[6] Shirai K, Horii J, Fujimori T (2021) Optimal sliding force characteristics of friction dampers for seismic response control of building structures considering sway-rocking motion. Soil Dynamics and Earthquake Engineering, 149, 106892.
https://doi.org/10.1016/j.soildyn.2021.106892

[7] Shirai K, Inoue N (2014) A seismic response estimation method for RC structures using random vibration theory. Journal of Advanced Concrete Technology, 12(2), 62–72.
https://doi.org/10.3151/jact.12.62

[8] Shirai K, Park J (2020) Use of scrap tire pads in vibration control system for seismic response reduction of buildings. Bulletin of Earthquake Engineering, 18(5), 2497–2521.
https://doi.org/10.1007/s10518-020-00787-2

[9] Takeda T (1974) Dynamic calculation for reinforced concrete buildings. Concrete Journal, 12(8), 33–41. (in Japanese)
https://doi.org/10.14826/coj1963.12.8_33

Chapter VI

Conclusions and recommendations

Conclusions and recommendations

1. Conclusions

The following conclusions can be drawn from this study:

(1) A system for controlling vibration of structures caused by earthquakes using scrap tire pads (STPs) has been proposed. The applicability of the proposed system was evaluated through a simple estimation of the number of tires required to apply the proposed system to buildings.
(2) Vertical loading tests on the STP unit specimens confirmed that it could withstand a certain amount of vertical compressive pressure without failure.
(3) Horizontal loading tests under constant vertical pressure were performed to confirm and demonstrate the behavior of the STP unit specimens. Stable and thick hysteretic loops of the STP unit specimens were observed, which confirms that it has a certain damping capacity without the installation of other energy absorbing devices.
(4) The horizontal equivalent stiffness and viscous damping coefficients of the STP specimens were identified, and all models showed similar tendencies, regardless of the tire mileage or manufacturer. The 30-cycle cyclic loading experiments showed no significant changes without failures.
(5) A seismic response analysis was performed on a simplified linear model with the application of a seismic mass damper (SMD) system utilizing STPs. The applied model showed useful reduction performance compared to the model without the system, proving the effectiveness of the proposed damper system.
(6) The seismic vibration response according to the presence or absence of the SMD system using STP was simulated using nonlinear building models, and it was found that the story drift response in the superstructure was reduced for models with the system installed. By using an approach to adopt reduced lateral stiffness and damping coefficients for the mass damper story, the nonlinearity of the

mainframe of the superstructure may be able to be considered and the control effectiveness may be improved.

2. Recommendations for the future study

This paper discusses STPs are utilized in the SMD system to control the vibration response of structures. Some of the tasks that were not covered in this study and require further research are listed below:

(1) A more detailed classification of used tires and new tires should lead to improved investigations into the effects of degradation and the characteristic change of STPs. It is necessary to distinguish between aging, where tires have been chemically affected over time, and using, which is mechanically affected by wear and compression through practical use.
(2) A study of used tires with much greater mileage (e.g., 50,000 km) than the tires used in this study should be carried.
(3) For the prediction of the approximate service time of SMD systems using STPs, an investigation of the limitation characteristics of STPs should be carried.
(4) For improved performance over the SMD system utilizing STPs analyzed in this study, systems coupled with other dampers and seismic bracing, or seismic isolation devices, should be suggestible and their performance also should be examined.
(5) Response analysis considering three-dimensional effects including vertical, rotational, or torsional behavior of STP units should be conducted.
(6) The failure limit characteristics of the SMD system should be investigated when the slip between the STP unit and the upper and lower slabs is taken into account through the method of securing the STP unit without adhesion.

LIST OF RELATED PUBLISHED PAPERS

- International peer-reviewed journal

(1) Park J, Shirai K, Kikuchi M (2022) A seismic mass damper system using scrap tire pads: Loading tests on mechanical properties and numerical assessment of the response control effects, Soil Dynamics and Earthquake Engineering, vol. 157, 107257. https://doi.org/10.1016/j.soildyn.2022.107257

(2) Shirai K, Park J (2020) Use of scrap tire pads in vibration control system for seismic response reduction of buildings, Bulletin of Earthquake Engineering, 18(5), 2497–2521. https://doi.org/10.1007/s10518-020-00787-2

- International peer-reviewed conference proceedings

(1) Park J, Shirai K, Kikuchi M (2020) A seismic mass damper using scrap tire pads: experiment on mechanical property and analysis of control effect. The 17th World Conference on Earthquake Engineering, Sendai, Japan.

- Domestic conference proceedings

(1) Park J, Shirai K, Kikuchi M (2017) A proposal of a seismic mass damper system using waste tires appropriate for RC building structures part 3 Analyzing Experimental Data and Earthquake Response Analysis, Summaries of technical papers of Annual Meeting Architectural Institute of Japan, B-2, 745-746. (In Japanese)

(2) Park J, Shirai K, Kikuchi M (2018) A proposal of a seismic mass damper system using waste tires appropriate for RC building structures part 4 Experimental Results of Different STP specimens", Summaries of

technical papers of Annual Meeting Architectural Institute of Japan, B-2, 353-354. (In Japanese)
(3) Park J, Shirai K, Kikuchi M (2019) A proposal of a seismic mass damper system using waste tires appropriate for RC building structures part 5 earthquake response analysis using nonlinear MDOF models, Summaries of technical papers of Annual Meeting Architectural Institute of Japan, B-2, 197-198.
(4) Shirai K, Park J, Kikuchi M (2017) A proposal of a seismic mass damper system using waste tires appropriate for RC building structures part 2 methods and results of loading tests on a STP specimen, Summaries of technical papers of Annual Meeting Architectural Institute of Japan, B-2, 743-744. (In Japanese)

- Theses

(1) Park J (2017) Study of the performance of a seismic mass damper system using waste tires -Loading test of rubber pad specimen-, Bachelor's thesis in Hokkaido University. (In Japanese)
(2) Park J (2019) Characteristic evaluation of tire rubber pads based on loading tests and performance examination of a seismic vibration control system by response analysis, Master's thesis in Hokkaido University. (In Japanese)